Effective field theory and global fits for Higgs physics at the LHC (and beyond)

Anke Biekötter

26.04.2019–10.05.2019

Contents

1 Standard Model effective field theory for the Higgs sector

The discovery of a scalar particle with a mass of $m_h = 125$ GeV at the LHC [1, 2] and subsequent precision analyses of this new boson suggest that it is indeed the Higgs boson of the Standard Model [3–5] or behaves very similar to it. Apart from confirming our ideas about the role of symmetries in theories of fundamental interactions, findings to date – or more so their absence – have led to a shift in the focus of experimental analyses [6]. Increasingly, targeted searches for new particles or effects relying on "smoking gun" signatures are replaced by more holistic precision tests of Standard Model dynamics in ever more extreme phase space regions. Confronted with a large abundance of models describing new physics at the TeV-scale on the one side and a plethora of experimental precision measurements on the other side, our aim is to describe deviations from the Standard Model expectations in a model independent and reproducible way. A framework apt to address this challenge of a comprehensive description of new physics is effective field theory (EFT) [7–11]. In Higgs physics, effective field

theories can be used to model the low energy effects of TeV-scale theories, describing not only small deviations from the SM couplings in magnitude, but also modifications of their Lorentz structures.

This chapter is loosely based on Refs. [12, 13] and is organized as follows: We will first introduce the Higgs sector of the SM in Section 1.1 to establish the notations and give an overview of the dominant Higgs-production modes at the LHC and its decays. In Section 1.2, we will introduce the EFT framework from the top-down using Fermi's theory of the muon decay as an example. Then, in Section 1.3 we will take the opposite approach and construct a basis of dimension-six operators from the bottom up. We will discuss the phenomenology of the dimension-six operators relevant for Higgs physics in Section 1.4 and describe the relevant physical processes constraining our set of dimension-six operators in Section 1.5. In Section 1.6, we will introduce the Δ–framework as an alternative approach to describe deviations from the SM Higgs couplings.

1.1 The Higgs sector of the Standard Model

The electroweak sector of the SM is described as a gauge theory with an $SU(2)_L \times U(1)_Y$ symmetry [14–17] which is broken to $U(1)_Q$ by the presence of the scalar $SU(2)_L$ Higgs doublet ϕ [3–5]. The SM Higgs sector is described by the following Lagrangian

$$\begin{aligned}
\mathcal{L}_{\text{Higgs}} &= (D_\mu \phi)^\dagger (D^\mu \phi) - V(\phi) + \mathcal{L}_{\text{Yukawa}} \,, \\
V(\phi) &= \mu^2 \phi^\dagger \phi + \lambda (\phi^\dagger \phi)^2 \,, \\
\mathcal{L}_{\text{Yukawa}} &= - \sum_{\text{generations}} \left(y_u \begin{pmatrix} \bar{u} \\ \bar{d} \end{pmatrix}_L \tilde{\phi}\, u_R + y_d \begin{pmatrix} \bar{u} \\ \bar{d} \end{pmatrix}_L \phi\, d_R + y_\ell \begin{pmatrix} \bar{\nu} \\ \bar{\ell} \end{pmatrix}_L \phi\, \ell_R + \text{h.c.} \right) \,,
\end{aligned} \tag{1}$$

with real parameters $\mu^2 < 0$ and λ in the Higgs potential, complex Yukawa couplings y_i which are matrices in flavor space and $\tilde{\phi} = i\sigma_2 \phi^*$. The covariant derivative is defined as

$$D_\mu \phi = \left(\partial_\mu + i g \frac{\sigma^a}{2} W_\mu^a + i \frac{g'}{2} B_\mu \right) \,, \tag{2}$$

with W_μ^a and B_μ denoting the gauge bosons of the $SU(2)_L$ and $U(1)_Y$ gauge groups their respective coupling constants g and g' and σ^a being the Pauli matrices. The Higgs doublet can be written in terms of the physical Higgs field h, the vacuum expectation value (vev) of the Higgs potential $v = -\sqrt{\mu^2/\lambda}$ and the would-be Goldstone bosons w^i resulting from the spontaneous symmetry breaking [18, 19] of the electroweak sector as

$$\phi = \frac{1}{\sqrt{2}} \begin{pmatrix} -w^2 - i w^1 \\ v + h + i w^3 \end{pmatrix} \,. \tag{3}$$

The Goldstone bosons provide the longitudinal degrees of freedom of the massive gauge bosons and we can write the Higgs doublet in the Lagrangian in Eq. (1) in unitary gauge $\phi = \frac{1}{\sqrt{2}}(0,\, v+h)^T$. With this replacement we directly see that the same terms that induce the couplings of fermions and the weak bosons to the Higgs will also generate their masses. Therefore, there is a proportionality between the couplings of the Higgs boson to other SM particles x (which obtain their masses via electroweak symmetry breaking) and their masses $g_x \sim m_x$. The triple and quartic couplings of the Higgs boson are proportional to the parameter λ, rendering those couplings sensitive to the structure of the Higgs potential in Eq. (1).

Higgs production and decays

As the Higgs boson predominantly couples to heavy particles, its dominant production modes involve the top quark and the weak Z and W bosons. At the LHC, the main production processes of the Higgs boson are gluon fusion (ggF), weak boson fusion (WBF), associated production with a Z or W boson and production in association with a pair of top quarks. The Feynman diagrams for the dominant

(single) Higgs production modes at the LHC are shown in (the upper panel of) Fig. 1. We list their production cross section at a $\sqrt{s} = 13\,\text{TeV}$ pp-collider in Tab. 1.

We can probe the Higgs self-coupling λ and obtain insight on the structure of the Higgs potential in Eq. (1) by measuring di-Higgs production. The relevant Feynman diagrams for this process are given in the lower row of Fig. 1. Di-Higgs production is not only phase space suppressed by the mass of the Higgs bosons, it suffers in addition from the negative interference between the two diagrams, rendering its cross section accidentally small. In fact, its cross section is around a factor 17 smaller than for Higgs production in association with a top quark pair, see Tab. 1, despite the fact that $t\bar{t}h$ production suffers from an even stronger phase space suppression and di-Higgs production only involves one additional coupling of $\lambda \sim 0.13$ or $y_t \sim 0.7$. The strong negative interference of the two diagrams contributing to di-Higgs production makes this process especially sensitive to new physics with modified Higgs sectors which might reduce such cancellations and enhance its cross section.

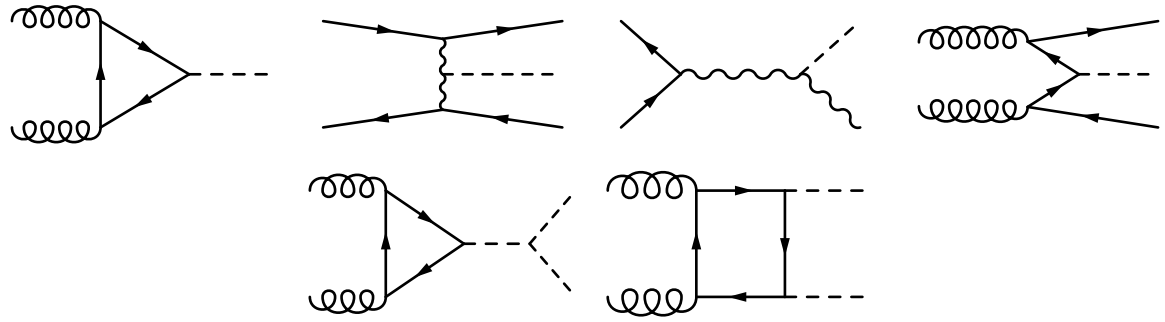

Figure 1: Feynman diagrams of the dominant production modes of the Higgs boson at the LHC. Upper row: gluon fusion (left), weak boson fusion (middle left), associated production with a weak boson (middle right) and $t\bar{t}h$ production (right). Lower row: Di-Higgs production.

production channel	cross section [pb]
ggF	48.58
WBF	3.782
Wh	1.373
Zh	0.8839
tth	0.5071
hh	0.03105

Table 1: Production channels of the Higgs boson and their SM cross section predictions for LHC Run II ($\sqrt{s} = 13\,\text{TeV}$) [20].

Since the Higgs boson couples to all massive particles of the SM, it has a broad spectrum of decay modes. It prefers to decay into a pair of the heaviest particles allowed by phase space which is a pair of bottom quarks, see Fig. 2. The decay to a pair of Z or W bosons is suppressed by one of the bosons having to be off-shell due to their masses. The decay of a Higgs boson to a pair of gluons, photons or $Z\gamma$ is only possible via loop diagrams. Given the large QCD backgrounds at a hadron collider, the dominant (hadronic) decay modes of the Higgs boson are not the most sensitive experimental signatures. Despite their low branching ratios of 0.2 % and 0.3 % respectively, the di-photon $\gamma\gamma$ and $ZZ^* \to 4\ell$ decay modes of the Higgs boson are considered its *golden channels*.

1.2 Effective field theory

Effective field theory provides a flexible and theoretically sound framework to describe new physics in an (almost) model independent way [6]. It is based on the assumption of a hierarchy of scales, i. e. the idea that new physics appears at a scale Λ much larger than the scale of the physical process E under

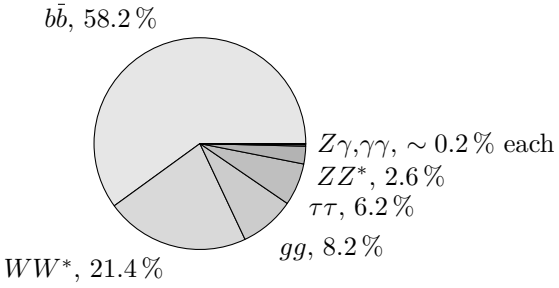

Figure 2: SM predictions for the branching ratios of the Higgs boson [20].

consideration (and accessible by experiments). An effective field theory aims at describing all effects relevant at a given scale, while neglecting those which only play a role at a significantly different scale. Applied to particle physics, this means that an effective field theory describes the effects of new particles and structures at an energy scale where these can not (yet) be resolved. Heavy degrees of freedom of a new physics theory are integrated out and their low-energy effects are described by fixing the (propagating) particle content and the underlying symmetry structure and constructing new operators with mass-dimension $d > 4$ from it.
As the action $S = \int \mathrm{d}^4x\, \mathcal{L}(x)$ of a quantum field theory is dimension-less, all terms in a Lagrangian need to have mass dimension $d = 4$. Therefore, in an effective field theory all operators of mass dimension $d > 4$ need to be suppressed by powers of a (new physics) scale Λ which is usually assumed to be universal. The Lagrangian of an effective field theory is thus given by [7–11]

$$\mathcal{L}_{\mathrm{EFT}} = \sum_i \frac{c_i}{\Lambda^{d-4}} \mathcal{O}_i^{(d)}\,, \tag{4}$$

where c_i denote the Wilson coefficients corresponding to the higher-dimensional operators $\mathcal{O}_i$. The contribution of each operator $\mathcal{O}_i^{(d)}$ to amplitudes of physical processes at an energy scale of order $\mathcal{O}(E)$ has a maximum scaling of $(E/\Lambda)^{(d-4)}$. When we assume a large new physics scale Λ, this ratio is small $E/\Lambda \ll 1$ by construction and the effective field theory describes small deviations from the SM predictions, except for observables that vanish or are suppressed by small parameters within the SM [21]. Given a large new physics scale Λ, it is often justified to truncate the effective theory at a given dimension, typically dimension six for EFTs based on the SM field content, since higher-dimensional terms are suppressed and rendered irrelevant by additional powers of Λ.

An illustrative top down example for an effective theory, i. e. starting from a full, UV-complete new physics model and integrating out the heavy degrees of freedom, is Fermi's theory of the muon decay [22]. We display the corresponding Feynman diagrams in Fig. 3. At energy scales much lower than the mass of the W boson, $E \ll \Lambda = m_W$, the W boson can be integrated out and the decay of the muon is effectively described by a four-point interaction of fermions. This is equivalent to approximating the W boson propagator in the decay for low momenta p

$$\frac{g^2}{p^2 - m_W^2} \quad \to \quad \frac{g^2}{m_W^2}\,, \tag{5}$$

which at an energy scale of the mass of the muon is a very good approximation $m_\mu^2/m_W^2 \approx 10^{-6}$. The effective Lagrangian of the Fermi theory of the muon decay in terms of a dimension-six operator reads [21]

$$\mathcal{L}_{\mathrm{EFT}} \supset c^{(6)} \left(\bar{e}\gamma_\alpha P_L \nu_e\right)\left(\bar{\nu}_\mu \gamma^\alpha P_L \mu\right) + \mathrm{h.c.}, \qquad c^{(6)} = -\frac{g^2}{2m_W^2} = -\frac{2}{v^2}\,. \tag{6}$$

At energies $E \ll m_W$, this four-point contact interaction of the muon decay is a valid approximation for the full electroweak process described by the SM.

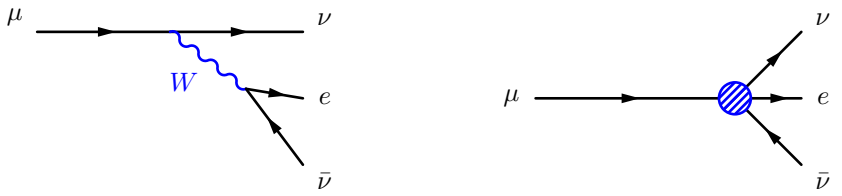

Figure 3: The muon decay as described by the full theory of weak interactions (left) and by an effective theory after integrating out the W boson (right).

1.3 Constructing SMEFT from the bottom-up

In the previous section, we have seen the textbook example for the construction of a top-down EFT, the Fermi theory of the muon decay. Starting from a full theory, in this case the electroweak sector of the SM, we have constructed an effective low-energy description of this theory, valid for $E < m_W$, describing the muon decay with an effective four-fermion operator at dimension six.

In this section, we want to go the opposite way and construct an effective field theory bottom-up. If we restrict ourselves to the field content of the SM, the only operator that we can construct at dimension five is the *Weinberg operator* $(\bar{L}_L\tilde{\phi}^*)(\tilde{\phi}^\dagger L_L)$ which, however, violates lepton number conservation. Consequently, if we want to preserve baryon and lepton number conservation, operators need to be at least of dimension six. Our aim for this section is to construct a complete basis of operators based only on the following five assumptions:

1. **Field content:** We will build new operators from the SM fields only.
2. **Symmetries:** We will only allow operators which are invariant under the SM gauge group $SU(3)_C \times SU(2)_L \times U(1)_Y$ and under proper orthochronous Poincaré transformations. In addition, we require lepton and baryon number conservation.
3. **Counting scheme:** We only keep operators up to mass dimension six.
4. **Flavor:** We assume a universal flavor structure, i. e. we will not distinguish between the different fermion families.
5. **Higgs sector:** We assume the Higgs boson h and the would-be Goldstone bosons to form an $SU(2)_L$ doublet as given in Eq. (3), limiting ourselves to SM EFT (or *linear EFT*) in contrast to *non-linear Higgs EFT* which is often simply denoted *Higgs EFT* (HEFT).

Respecting those assumptions and barring Hermitian conjugation, we can construct 59 operators [7–11, 23–29] and our effective Lagrangian is given by

$$\mathcal{L}_{\text{EFT}} = \mathcal{L}_{\text{SM}} + \sum_i^{59} \frac{c_i}{\Lambda^2}\mathcal{O}_i^{(6)} \,. \tag{7}$$

The definition of an operator basis is not unique, as operators can be translated into one another using field redefinitions, Fierz identities and integration by parts. Popular basis choices include the *Warsaw* basis, the *Strongly interacting Little Higgs* (SILH) basis and the *Hagiwara-Ishihara-Szalapski-Zeppenfeld* (HISZ) basis. Here, we will use a convention based on the latter and will follow the approach of Ref. [30,31] for its definition, starting from a larger set of operators and explicitly using the equations of motion to remove operators with blind directions to electroweak precision data.

We can classify the 59 operators in our basis according to their field content in terms of gauge fields strength tensors X, Higgs doublet ϕ and fermion fields ψ as well as derivatives ∂/D and their properties. In the following, we will list the categories of dimension-six operators and restrict ourselves to a subset of those which we will discuss in more detail. We can loosely classify the operators into two sets, see Tab. 2: operators containing bosonic fields only (17 operators) and those containing fermionic fields as well (42 operators).

bosonic		#	fermionic		#
gauge only	X^3	2	4-fermion	ψ^4	25
Higgs only	ϕ^6, $\phi^4\partial^2$	2	Higgs-fermion	$\phi^3\psi^2$	3
Higgs-gauge	ϕ^2X^2, ϕ^2XD^2	(8) 7	Higgs-gauge-fermion	$\phi^2\psi^2D$	(8) 6
CP-odd	$\phi^2X\tilde{X}$, $\phi^2\tilde{X}D^2$	6	dipole	$\phi\psi^2X$	8

Table 2: Overview of dimension-six operator ordered by field content and structure. We have grayed out operators which are mostly irrelevant for Higgs physics. We also list the number of operators of a given structure (before using the equations of motion).

Out of the 17 purely bosonic operators, 6 are CP violating. We will refer to them as ϕ^2X^2 and ϕ^2XD^2 or $\phi^2X\tilde{X}$ and $\phi^2\tilde{X}D^2$ using the tilde to denote the dual field strength. The remaining CP-even operators can further be subclassified into operators containing gauge fields only (X^3, 2 operators), operators containing the Higgs field only (ϕ^6 and $\phi^4\partial^2$, 2 operators) and operators consisting of both gauge and Higgs fields (ϕ^2X^2 and ϕ^2XD^2, 7 operators). The set of fermionic operators consists of 4-fermion operators (ψ^4, 25 operators), operators containing fermions and the Higgs ($\phi^3\psi^2$, 3 operators), fermionic Higgs-gauge operators ($\phi^2\psi^2D$, 6 operators) and fermionic Higgs-gauge operators with a tensor Lorentz structure ($\phi\psi^2X$, 8 operators) which we will also refer to as dipole operators.

Not all of the operators in Tab. 2 are relevant for Higgs physics and we will therefore only consider a subset of them in the following. Since we expect CP violation to be measured in a dedicated analysis rather than a global fit [32, 33], we restrict the set of operators to the P-even and C-even ones and only list CP-odd operators in Eq. (56) for completeness. We also neglect all operators describing four-fermion contact interactions except $\mathcal{O}_{LLLL}$ defined in Eq. (13). 4-fermion operators do not contribute to any of the main Higgs-production modes, see Section 1.1, and we only keep $\mathcal{O}_{LLLL}$ because of its influence on the well measured Fermi constant G_F which is relevant for our study of electroweak precision data in Section 1.5. Dipole operators flip the fermion chirality due to their Lorentz structure. Their interference with the SM amplitudes is hence small. As they are also expected to be suppressed by the fermion Yukawa, we will generally neglect all dipole operators except $\mathcal{O}_{tG}$ which we will come back to in Eq. (15). For current constraints on dipole operators involving light or heavy quarks see e. g. Refs. [34–36].

We will now discuss the bosonic, Higgs-fermion and Higgs-gauge fermion operators in more detail, focussing especially on the vertices they are contributing to. In Section 1.4, we will focus on the phenomenology of the operators on the Lagrangian level and then discuss processes which are capable of setting meaningful limits on those in Section 1.5.

Bosonic operators

We start our discussion of the dimension-six operators by listing the operators containing Higgs or gauge fields only. There are six CP-odd bosonic operators in our basis, see to Eq. (56), which we neglect in our analysis. We explicitly write down 12 CP-conserving operators and will later use the equations of motion, Eq. (14), to remove one of them. There are two operators which consist of gauge fields only

$$\mathcal{O}_{WWW} = \mathrm{Tr}\left(\hat{W}_{\mu\nu}\hat{W}^{\nu\rho}\hat{W}_{\rho}^{\mu}\right) \qquad \mathcal{O}_G = f_{abc}G_{a\nu}^{\rho}G_{b\lambda}^{\nu}G_{c\rho}^{\lambda} \tag{8}$$

and eight operators containing Higgs and gauge fields

$$\begin{aligned}
\mathcal{O}_{GG} &= \phi^\dagger\phi\, G^a_{\mu\nu}G^{a\mu\nu} & \mathcal{O}_W &= (D_\mu\phi)^\dagger\hat{W}^{\mu\nu}(D_\nu\phi) & \mathcal{O}_{\phi1} &= (D_\mu\phi)^\dagger\phi\,\phi^\dagger D^\mu\phi \\
\mathcal{O}_{WW} &= \phi^\dagger\hat{W}_{\mu\nu}\hat{W}^{\mu\nu}\phi & \mathcal{O}_B &= (D_\mu\phi)^\dagger\hat{B}^{\mu\nu}(D_\nu\phi) & \mathcal{O}_{\phi4} &= \phi^\dagger\phi\,(D_\mu\phi)^\dagger D^\mu\phi \\
\mathcal{O}_{BB} &= \phi^\dagger\hat{B}_{\mu\nu}\hat{B}^{\mu\nu}\phi & \mathcal{O}_{BW} &= \phi^\dagger\hat{B}_{\mu\nu}\hat{W}^{\mu\nu}\phi\,.
\end{aligned} \tag{9}$$

The covariant derivative acting on the Higgs is defined in Eq. (2) and the hatted field strengths are rescaled with extra coupling factors $\hat{B}_{\mu\nu} = ig'B_{\mu\nu}/2$ and $\hat{W}_{\mu\nu} = ig\sigma^a W^a_{\mu\nu}/2$ to ensure that they contribute to vertices with the same coupling orders as their SM counterparts. This rescaling is motivated by our expectations from known UV-completions. It has, however, no effect on our analysis or its interpretation. Two operators contain the Higgs field only

$$\mathcal{O}_{\phi 2} = \frac{1}{2}\partial^\mu(\phi^\dagger\phi)\partial_\mu(\phi^\dagger\phi) \qquad \mathcal{O}_{\phi 3} = -\frac{1}{3}(\phi^\dagger\phi)^3 \tag{10}$$

The effect of the operators in Eqs. (8)-(10) on Higgs and gauge interactions is summarized in Tab. 3. All operators in Eqs. (9) and (10) affect Higgs interactions. Moreover, many of the operators in Eq. (9)

operator	$Hf\bar{f}$	HHH	HVV	VVV
$\mathcal{O}_{\phi 1}$	×	×	×	×
$\mathcal{O}_{\phi 2}$	×	×	×	
$\mathcal{O}_{\phi 3}$		×		
$\mathcal{O}_{\phi 4}$	×	×	×	
$\mathcal{O}_{WW}$			×	
$\mathcal{O}_{BB}$			×	
$\mathcal{O}_{W}$			×	×
$\mathcal{O}_{B}$			×	×
$\mathcal{O}_{BW}$			×	×
$\mathcal{O}_{WWW}$				×

Table 3: List of bosonic operator and their effect on couplings. Some of the operators also contribute to $HHHH$, $HVVV$, $HHVV$ or $VVVV$, but we limit ourselves to a list of interactions that is phenomenologically relevant for the processes studied in the following.

and the operator $\mathcal{O}_{WWW}$ lead to anomalous triple gauge couplings and can therefore be constrained using diboson measurements. We will discuss this source of constraints in more detail in Section 1.5. For a more detailed discussion of the bosonic operators, including an analysis of their (non-SM) Lorentz structures, see Ref. [31, 37–39]. We will discuss the limits on the operator $\mathcal{O}_G$ in Eq. (12) in Section 3. Some of the operators in Eq. (9) contribute to the two-point functions of the electroweak gauge bosons. For the operators $\mathcal{O}_{WW}$ and $\mathcal{O}_{ZZ}$ these additional contributions can be removed by a trivial redefinition of the fields and couplings. For $\mathcal{O}_{\phi 1}$ and $\mathcal{O}_{BW}$ however, the situation is more involved and their additional contributions to the kinetic terms or mass terms of the electroweak gauge bosons cannot be fully removed by redefinitions of the fields, as explained e. g. in Ref. [31]. The operator $\mathcal{O}_{BW}$ contributes to W^3–B mixing, while the operator $\mathcal{O}_{\phi 1}$ contributes to the Z boson mass, but not the W boson mass. They are therefore constrained by the S oblique parameter and $\Delta\rho$, or the T oblique parameter, respectively [40, 41]. We will discuss electroweak precision data as a source of constraints on dimension-six operators in Section 1.5. The operator $\mathcal{O}_{\phi 2}$ contributes to the kinetic term of the Higgs field and requires a redefinition of the field, if we want to keep the canonical form of the kinetic term. We will discuss its phenomenology, a global shift of the Higgs couplings to other particles and the introduction of a momentum-dependent Higgs self-coupling, in Section 1.4. The operator $\mathcal{O}_{\phi 3}$ is particularly relevant because of its modification of the Higgs potential. We will come back to it in Section 4, when we are including the Higgs self-coupling in a global fit. Using the equations of motion for the Higgs and gauge bosons [10] will allow us to remove three operators from our basis, see Eq. (14). To avoid blind directions to electroweak precision data [30, 31], we will later choose to remove $\mathcal{O}_{\phi 4}$ from our set of operators.

Fermionic operators

After the discussion of operators involving only the Higgs and the electroweak gauge fields, we will now study a second group of operators containing fermionic (and bosonic) fields. We will distinguish

between operators containing fermions and the Higgs only, operator containing fermions, the Higgs and gauge fields with SM-like Lorentz structures, four-fermion operators and finally dipole operators, containing fermions, the Higgs and gauge fields and non-SM like Lorentz structures.

We begin with fermionic operators affecting the coupling of the Higgs to fermions and result in Yukawa-like interactions. Restricting ourselves to the third family of fermions, there are three such operators

$$\mathcal{O}_{e\phi,33} = \phi^\dagger\phi\, \bar{L}_3\phi e_{R,3} \qquad \mathcal{O}_{u\phi,33} = \phi^\dagger\phi\, \bar{Q}_3\tilde{\phi} u_{R,3} \qquad \mathcal{O}_{d\phi,33} = \phi^\dagger\phi\, \bar{Q}_3\phi d_{R,3} \tag{11}$$

In addition we consider the group of fermionic Higgs-gauge operators. Assuming flavor universality, we start from a list of eight operators and will reduce their number to six using the equations of motion

$$\begin{aligned}
\mathcal{O}^{(1)}_{\phi Q} &= \phi^\dagger (i\overleftrightarrow{D}_\mu \phi)(\bar{Q}\gamma^\mu Q) & \mathcal{O}^{(3)}_{\phi Q} &= \phi^\dagger (i\overleftrightarrow{D}^a_\mu \phi)(\bar{Q}\gamma^\mu \frac{\sigma_a}{2} Q) \\
\mathcal{O}^{(1)}_{\phi L} &= \phi^\dagger (i\overleftrightarrow{D}_\mu \phi)(\bar{L}\gamma^\mu L) & \mathcal{O}^{(3)}_{\phi L} &= \phi^\dagger (i\overleftrightarrow{D}^a_\mu \phi)(\bar{L}\gamma^\mu \frac{\sigma_a}{2} L) \\
\mathcal{O}^{(1)}_{\phi u} &= \phi^\dagger (i\overleftrightarrow{D}_\mu \phi)(\bar{u}_R\gamma^\mu u_R) \\
\mathcal{O}^{(1)}_{\phi d} &= \phi^\dagger (i\overleftrightarrow{D}_\mu \phi)(\bar{d}_R\gamma^\mu d_R) \\
\mathcal{O}^{(1)}_{\phi e} &= \phi^\dagger (i\overleftrightarrow{D}_\mu \phi)(\bar{e}_R\gamma^\mu e_R) \\
\mathcal{O}^{(1)}_{\phi ud} &= \tilde{\phi}^\dagger (i\overleftrightarrow{D}_\mu \phi)(\bar{u}_R\gamma^\mu d_R)
\end{aligned} \tag{12}$$

The operator $\mathcal{O}^{(1)}_{\phi ud}$ contains the charged current $\bar{u}_R\gamma^\mu d_R$ [42–45]. Given the known flavor physics constraints and the fact that it has no equivalent Standard Model structure to interfere with, we will ignore it in our analyses.

An important phenomenological consequence of the operators in Eq. (12) is the generation of anomalous weak boson couplings to fermions, see Tab. 4. In this table, we have also included the bosonic operators $\mathcal{O}_{\phi 1}$ and $\mathcal{O}_{BW}$ because of their influence on weak boson couplings to fermions after the field redefinitions. The operators in Eq. (12) leave the Higgs coupling to fermions unchanged. They do, however, introduce point-like $HVff$ interactions and therefore contribute to Higgs production in association with an electroweak boson, see also the discussion in Sec. 3.

25 of the 59 dimension-six operators describe four-fermion contact interactions. Here, we only consider one of them, as it induces a shift in the Fermi constant and is therefore relevant for the description of electroweak precision data

$$\mathcal{O}_{LLLL} = (\bar{L}_1\gamma_\mu L_2)\,(\bar{L}_2\gamma^\mu L_1)\,. \tag{13}$$

The equations of motion [10] for the Higgs field and the electroweak gauge fields provide equivalence

	$Hf\bar{f}$	Zqq	Wqq'	$HZqq$	$HWqq'$	$Zl\bar{l}$	$Wl\nu$
$\mathcal{O}_{\phi 1}$	×	×	×			×	×
$\mathcal{O}_{BW}$		×	×			×	×
$\mathcal{O}^{(3)}_{\phi Q}$		×	×	×	×		
$\mathcal{O}^{(1)}_{\phi Q}$		×		×			
$\mathcal{O}^{(1)}_{\phi u}$		×		×			
$\mathcal{O}^{(1)}_{\phi d}$		×		×			
$\mathcal{O}^{(1)}_{\phi e}$						×	

Table 4: List of operators affecting electroweak precision observables and their effect on fermionic couplings testable at the LHC.

relations between (the sums of) dimension-six operators that allow us to eliminate three operators from the set that we have defined so far [12, 13]

$$
\begin{aligned}
2\mathcal{O}_{\phi 2} + 2\mathcal{O}_{\phi 4} &= \left(y^e_{33}(\mathcal{O}_{e\phi,33})^\dagger + y^u_{33}\mathcal{O}_{u\phi,33} + y^d_{33}(\mathcal{O}_{d\phi,33})^\dagger + \text{h.c.}\right) - \frac{\partial V(h)}{\partial h} \\
2\mathcal{O}_B + \mathcal{O}_{BW} + \mathcal{O}_{WW} + g^2\left(\mathcal{O}_{\phi 4} - \frac{1}{2}\mathcal{O}_{\phi 2}\right) &= -\frac{g^2}{4}\sum_{\text{flavor}}\left(\mathcal{O}^{(3)}_{\phi L} + \mathcal{O}^{(3)}_{\phi Q}\right) \\
2\mathcal{O}_B + \mathcal{O}_{BW} + \mathcal{O}_{BB} + g'^2\left(\mathcal{O}_{\phi 1} - \frac{1}{2}\mathcal{O}_{\phi 2}\right) &= \\
&\quad - \frac{g'^2}{2}\left(-\frac{1}{2}\mathcal{O}^{(1)}_{\phi L} + \frac{1}{6}\mathcal{O}^{(1)}_{\phi Q} - \mathcal{O}^{(1)}_{\phi e} + \frac{2}{3}\mathcal{O}^{(1)}_{\phi u} - \frac{1}{3}\mathcal{O}^{(1)}_{\phi d}\right) . \qquad (14)
\end{aligned}
$$

We choose to eliminate the leptonic operators $\mathcal{O}^{(1)}_{\phi L}$ and $\mathcal{O}^{(3)}_{\phi L}$ and the bosonic operator $\mathcal{O}_{\phi 4}$ to avoid blind directions to electroweak precision data [30, 31] .

The last category of dimension-six operators that we want to discuss is that of *dipole operators*, fermionic Higgs-gauge operators with a tensor Lorentz structure. In the HISZ basis, there are eight such operators which we list explicitly in Eq. (58). Due to their non-SM Lorentz structure, their tree-level interference with the SM is helicity suppressed. In general, we will therefore not consider them in our analysis. In Chapter 3 we will however discuss the effect of the operator

$$\mathcal{O}_{tG} = (\bar{Q}\sigma^{\mu\nu}T^a u_R)\,\tilde{\phi}\,G^a_{\mu\nu} \qquad (15)$$

on $t\bar{t}h$ production. For bounds on dipole operators from partial–wave unitarity violation, the top sector or measurements of the electric and magnetic dipole moments see Refs. [34–36, 46].

This completes the discussion of the set of dimension-six operators included in our studies. Altogether, we have identified 21 operators which are potentially relevant for our study of Higgs physics

$$
\begin{aligned}
&\{\mathcal{O}_G,\, \mathcal{O}_{WWW},\, \mathcal{O}_{\phi 1},\, \mathcal{O}_{\phi 2},\, \mathcal{O}_{\phi 3},\, \mathcal{O}_{GG},\, \mathcal{O}_{WW},\, \mathcal{O}_{BB},\, \mathcal{O}_{BW},\, \mathcal{O}_B,\, \mathcal{O}_W\} \quad \text{bosonic} \\
&\left\{\mathcal{O}_{u\phi,33},\, \mathcal{O}_{d\phi,33},\, \mathcal{O}_{e\phi,33},\, \mathcal{O}^{(3)}_{\phi Q},\, \mathcal{O}^{(1)}_{\phi u},\, \mathcal{O}^{(1)}_{\phi d},\, \mathcal{O}^{(1)}_{\phi e},\, \mathcal{O}^{(1)}_{\phi Q},\, \mathcal{O}_{tG},\, \mathcal{O}_{LLLL}\right\} \quad \text{fermionic,} \qquad (16)
\end{aligned}
$$

with the operator definitions given in Eqs. (9)–(12). We will later discuss in Section 3 how additional precision constraints from multi-jet production and the top sector on the operators $\mathcal{O}_G$ and $\mathcal{O}_{tG}$ respectively and the current reach for $\mathcal{O}_{\phi 3}$ at the LHC will render them irrelevant for current global studies of the Higgs sector at 13 TeV. The maximum number of operators included in our LHC Higgs fits is therefore 18 operators. In addition, we will include an invisible Higgs branching ratio as an additional free parameter.

1.4 Phenomenology of dimension-six operators

In this section, we want to examine the phenomenology of new interactions induced by dimension-six operators in more detail. Starting from a short summary of the vertices and field shifts of dimension-six operators, we will take the operator $\mathcal{O}_{\phi 2}$ as an example and study its effects explicitly.

A first, obvious result of dimension-six operators is the introduction of new vertices with higher-order contact interactions. We have already seen this effect in our analysis of Fermi's theory example in Section 1.2 in the form of a four-fermion vertex not present in the SM. Besides, dimension-six operators can also contribute to vertices already present at dimension-four: For two operators with dimension d and $d+2$ to contribute to the same vertex at tree-level, they need to have the same field content after electroweak symmetry breaking. To achieve this, the higher-dimensional operator must either contain two additional powers of the Higgs doublet or two more derivatives compared to its lower-dimensional

counter part. The vertices thus obtain additional contributions which can roughly be described as [21], respectively,

$$\frac{v^2}{\Lambda^2} \qquad \text{or} \qquad \frac{p^2}{\Lambda^2}\,. \tag{17}$$

The first type of operators with a v^2 proportionality will leave the Lorentz structure of the vertex unchanged and only contribute to the total rate without influencing the kinematics of the interaction. This is true, for instance, for the fermionic operators with Higgs couplings in Eq. 11. After electroweak symmetry breaking the operator $\mathcal{O}_{u\phi,33}$ leads to contribution of the form

$$\mathcal{O}_{u\phi,33} = \phi^\dagger\phi\;\bar{Q}_3\tilde{\phi}u_{R,3} \quad \rightarrow \quad v^2\;\bar{Q}_3\tilde{\phi}u_{R,3} \tag{18}$$

which has the exact same structure as the Yukawa terms in the SM Lagrangian in Eq. (1).

The second type of dimension-six operators, however, containing extra derivatives, will induce extra momentum dependences in a vertex. It will therefore change the kinematics of interactions and its effects will be more pronounced at high energies as we will shortly see for the contribution of the operator $\mathcal{O}_{\phi 2}$ to the Higgs self-interaction.

Finally, as we already discussed in Section 1.3, dimension-six operators can contribute to the two-point functions of the SM fields. In order to restore the canonical form of the kinetic terms, we therefore need to redefine our fields. This leads to global changes of the couplings of the physical fields or a change of their masses. Such changes are for instance induced by the operators $\mathcal{O}_{\phi 1}$, $\mathcal{O}_{\phi 2}$ and $\mathcal{O}_{BW}$.

The operator $\mathcal{O}_{\phi 2}$: As an example to show the effects of a dimension-six operator on two-point functions and kinematics, we will now study the phenomenology of the operator $\mathcal{O}_{\phi 2}$. It leads to a rescaling of all Higgs couplings and introduces new kinematic structures to the triple Higgs coupling. For convenience, we repeat its definition

$$\mathcal{L}_{\text{EFT}} = \mathcal{L}_{\text{SM}} + \frac{f_{\phi 2}}{\Lambda}\mathcal{O}_{\phi 2}\,, \qquad \mathcal{O}_{\phi 2} = \frac{1}{2}\partial^\mu(\phi^\dagger\phi)\partial_\mu(\phi^\dagger\phi). \tag{19}$$

In order to study the effects of $\mathcal{O}_{\phi 2}$ on the physical fields, we rewrite the products of the Higgs fields in unitary gauge by $\phi^\dagger\phi = (v^2 + 2v\tilde{h} + \tilde{h}^2)/2$ where we use $\tilde{h}$ for the Higgs field, because it is not yet a mass eigenstate. Explicitly writing out the SM contributions to the kinetic Higgs term and the Higgs self-coupling as given in Eq. 1, we obtain the following form for Eq. (19)

$$\begin{aligned}\mathcal{L}_{\text{EFT}} &\subset \frac{1}{2}\,\partial^\mu\tilde{h}\,\partial_\mu\tilde{h} - \lambda\left(v\,\tilde{h}^3 + \tilde{h}^4\right) + \frac{f_{\phi 2}}{8\Lambda^2}\,\partial^\mu\left(v^2 + 2v\tilde{h} + \tilde{h}^2\right)\,\partial_\mu\left(v^2 + 2v\tilde{h} + \tilde{h}^2\right) \\ &= \frac{1}{2}\left(1 + \frac{v^2 f_{\phi 2}}{\Lambda^2}\right)\partial^\mu\tilde{h}\,\partial_\mu\tilde{h} - \lambda v\tilde{h}^3 + \frac{v f_{\phi 2}}{\Lambda^2}\,\tilde{h}\,\partial^\mu\tilde{h}\,\partial_\mu\tilde{h} - \lambda\tilde{h}^4 + \frac{f_{\phi 2}}{2\Lambda^2}\,\tilde{h}^2\,\partial^\mu\tilde{h}\,\partial_\mu\tilde{h}.\end{aligned} \tag{20}$$

The first term of the above Lagrangian rescales the kinetic term of the Higgs boson by a factor $(1 + v^2 f_{\phi 2}/\Lambda^2)$ while the third and fifth term introduce new momentum-dependent triple and quartic Higgs self-couplings respectively. There are hence two important modifications of Higgs couplings due to the operator $\mathcal{O}_{\phi 2}$: First, a rescaling of the Higgs field $\tilde{h}$ is necessary to restore the canonical form of the kinetic term

$$h = \sqrt{1 + \frac{v^2 f_{\phi 2}}{\Lambda^2}}\;\tilde{h}, \tag{21}$$

which induces a universal shift of all couplings of the Higgs to other particles x

$$g_x = \frac{1}{\sqrt{1 + \frac{v^2 f_{\phi 2}}{\Lambda^2}}}\;g_x^{\text{SM}}\,. \tag{22}$$

The second important result is the appearance of a new Lorentz structure contributing to the triple (and quartic) Higgs self-coupling

$$6v\lambda \quad \rightarrow \quad 6v\lambda + 2v f_{\phi 2}\left(p_1\cdot p_2 + p_1\cdot p_3 + p_2\cdot p_3\right). \tag{23}$$

This new Lorentz structure will become relevant in Section 4 when we study the Higgs self-coupling at a potential 27 TeV upgrade of the LHC.

1.5 Constraining SMEFT operators

Having fixed the set of operators which we will consider for our analyses of the Higgs-gauge sector in the SMEFT framework, we now want to discuss the physical processes which will provide meaningful constraints on their Wilson coefficients. This includes rate measurements of different Higgs production and decay channels and of the diboson sector at the LHC, as well as electroweak precision observables at LEP.

Some of the operators in our set induce new Lorentz structures in vertices already present at dimension-four, as we have seen in the previous Section 1.4. They will therefore not only modify total rate measurements, but also influence differential distributions. Additional momentum-dependences of the dimension-six operators often renders (momentum-related) kinematic distributions the most powerful source of constraints for the Wilson coefficients of dimension-six operators.

Higgs sector

All of the operators in Eqs. (9)–(11) influence the couplings of the Higgs boson to other SM particles. In addition, the fermionic Higgs-gauge operators in Eq. (12) affect quark-induced Higgs production processes. We can therefore constrain their Wilson coefficients by measurements of the total rate of different Higgs production processes and Higgs decays. As all of the measurements of Higgs production with subsequent decays can potentially be affected by more than one dimension-six operator, the constraints on the Wilson coefficients of the operators will be correlated.

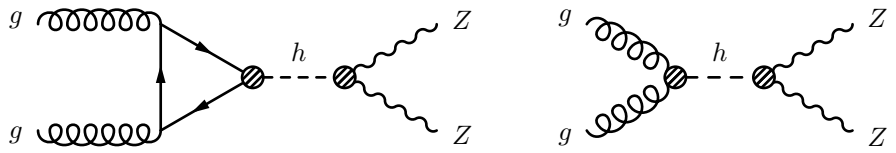

Figure 4: Feynman diagrams for the Higgs production and decay channel $pp \to h \to ZZ^*$. Blobs indicate the insertion of a dimension-six operator.

Let us consider for instance the channel $pp \to h \to ZZ^*$: On the production side, it is influenced by the operators $\mathcal{O}_{GG}$ and $\mathcal{O}_{u\phi,33}$, contributing to the hgg and $ht\bar{t}$ vertices respectively. The decay $h \to ZZ^*$ obtains modifications from all operators inducing hZZ vertices, i. e. from $\mathcal{O}_{BB}$, $\mathcal{O}_{WW}$, $\mathcal{O}_{B}$, $\mathcal{O}_{W}$, $\mathcal{O}_{BW}$, $\mathcal{O}_{\phi 1}$ and $\mathcal{O}_{\phi 2}$. In total, there are already nine operators influencing this one process, all of which contribute to other Higgs production or decay processes as well. This demonstrates the complexity of the correlations and motivates a global fit of all parameters and observables.

As a benchmark for current constraints on the Wilson coefficients of the considered dimension-six operators from the Higgs sector, we quote the typical reach of LHC Run I Higgs measurements

$$\frac{\Lambda}{\sqrt{|f|}} \gtrsim 250 \text{ ... } 500 \text{ GeV} \qquad \text{(pure Higgs analysis for LHC Run I [47])}. \tag{24}$$

Triple gauge vertices

Triple-gauge vertices (TGV) are probed at the LHC (and LEP) by studying di-boson production, specifically W^+W^- and WZ production, testing the structure of the WWZ or $WW\gamma$ vertices in kinematic distributions. Example Feynman diagrams for diboson production are given in Fig. 5. Some of the dimension-six operators in Eq. (9) contain VVV couplings and directly contribute to TGVs, inducing new Lorentz structures of the self-interactions of the electroweak gauge bosons. We can therefore use diboson production to constrain the Wilson coefficients of some of the bosonic operators in our basis, see Tab. 3. In addition to the modification of the self-interaction of electroweak gauge bosons by purely bosonic dimension-six operators, diboson production is also influenced by dimension-six

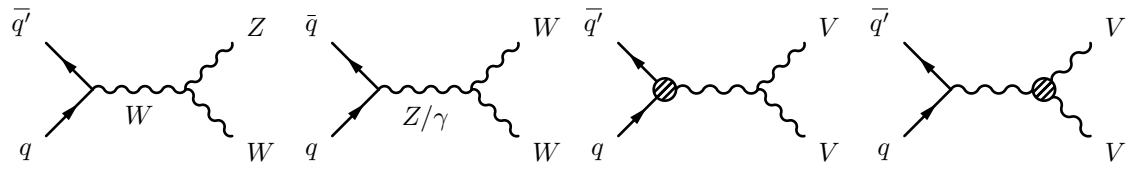

Figure 5: Feynman diagrams for diboson production at the LHC. From left to right: SM production of WZ and W^+W^-; contributions from dimension-six operators influencing $f\bar{f}V$ and VVV couplings.

operators with couplings $qq'V$ or $qq'VV$ on the production side at the LHC. The full set of dimension-six operators influencing di-boson production at the LHC is therefore given by

$$\begin{aligned}\mathcal{L}_{\text{EFT}} \supset & \frac{f_W}{\Lambda^2}\mathcal{O}_W + \frac{f_B}{\Lambda^2}\mathcal{O}_B + \frac{f_{BW}}{\Lambda^2}\mathcal{O}_{BW} + \frac{f_{\phi 1}}{\Lambda^2}\mathcal{O}_{\phi 1} + \frac{f_{WWW}}{\Lambda^2}\mathcal{O}_{WWW} \\ & + \frac{f_{\phi Q}^{(1)}}{\Lambda^2}\mathcal{O}_{\phi Q}^{(1)} + \frac{f_{\phi d}^{(1)}}{\Lambda^2}\mathcal{O}_{\phi d}^{(1)} + \frac{f_{\phi u}^{(1)}}{\Lambda^2}\mathcal{O}_{\phi u}^{(1)} + \frac{f_{\phi Q}^{(3)}}{\Lambda^2}\mathcal{O}_{\phi Q}^{(3)} \,. \end{aligned} \tag{25}$$

In the remaining part of this section, we want to focus on modifications of the gauge-boson self-interactions by bosonic dimension-six operators, i. e. those in the first line of the above Lagrangian, and the new Lorentz structures induced by them.

The deviations from the SM gauge couplings and the new coupling structures are historically written in terms of the parameters $\kappa_\gamma, \kappa_Z, g_1^Z, g_1^\gamma$, λ_γ, and λ_Z [48]. Fixing $g_1^\gamma = 1$ by using electromagnetic gauge invariance, the shifts are defined by

$$\begin{aligned}\Delta\mathcal{L}_{\text{TGV}} = & - ie\,(\kappa_\gamma - 1)\, W_\mu^+ W_\nu^- \gamma^{\mu\nu} - \frac{ie\lambda_\gamma}{m_W^2}\, W_{\mu\nu}^+ W^{-\nu\rho}\gamma_\rho^\mu - \frac{ig_Z\lambda_Z}{m_W^2}\, W_{\mu\nu}^+ W^{-\nu\rho} Z_\rho^\mu \\ & - ig_Z\,(\kappa_Z - 1)\, W_\mu^+ W_\nu^- Z^{\mu\nu} - ig_Z\,(g_1^Z - 1)\,\left(W_{\mu\nu}^+ W^{-\mu} Z^\nu - W_\mu^+ Z_\nu W^{-\mu\nu}\right) \,, \end{aligned} \tag{26}$$

where $e = gs_w$ and $g_Z = gc_w$. We can translate from one notational convention to the other using the relations

$$\begin{aligned}\kappa_\gamma &= 1 + \frac{g^2v^2}{8\Lambda^2}\,(f_W + f_B - 2f_{BW}) \\ \kappa_Z &= 1 + \frac{g^2v^2}{8c_w^2\Lambda^2}\left(c_w^2 f_W - s_w^2 f_B + \frac{4c_W^2 s_W^2}{c_W^2 - s_W^2} f_{BW}\right) - \frac{1}{4(c_W^2 - s_W^2)} f_{\phi 1}\frac{v^2}{\Lambda^2} \\ g_1^Z &= 1 + \frac{g^2v^2}{8c_w^2\Lambda^2}\left(f_W + 2\frac{s_W^2}{c_W^2 - s_W^2} f_{BW}\right) - \frac{1}{4(c_W^2 - s_W^2)} f_{\phi 1}\frac{v^2}{\Lambda^2} \\ \lambda_\gamma &= \lambda_Z = \frac{3g^2m_W^2}{2\Lambda^2} f_{WWW} \,. \end{aligned} \tag{27}$$

The appearance of extra derivatives in the new Lorentz structures of the self-couplings of the electroweak gauge bosons leads to additional momentum-dependences of the vertices compared to the SM ones. The analysis of (momentum-related) differential distributions will hence be crucial to constrain dimension-six operators using measurements of diboson production [30, 47].

For the more generic scenario of a non-linear or chiral effective Lagrangian [49–52], i. e. not assuming a doublet structure for the Higgs sector, the above parametrization would be extended and the correlations from gauge dependence are lost. Furthermore, the deviations generated by non-linear operators in the TGVs and the Higgs interactions could be completely de-correlated from one another. For the Higgs sector alone however, there exists a trivial mapping of the linear and non-linear analyses, as shown in Refs. [37, 38].

To get a very rough idea of the constraints that diboson production (in combination with measurements of the Higgs sector) can place on the Wilson coefficients f_B, f_W and f_{WWW}, we quote the typical reach of global Run I analyses,

$$\frac{\Lambda}{\sqrt{|f|}} \gtrsim 300 \text{ ... } 500 \text{ GeV} \qquad \text{(Higgs-gauge analysis for LHC Run I [47])}. \tag{28}$$

Measurements of TGVs were already performed at LEP. However, we note that already the LHC Run I di-boson measurements already clearly outperform the corresponding LEP measurements [47].

Electroweak precision data

The operators given in Eq. (12) affect the couplings of fermions to the weak gauge bosons, see Tab. 4. This is also true for some of the operators in Eq. (9), for which, however, the couplings to fermions only appear as a result of the redefinition of the fields to restore the canonical form of the kinetic terms. The full set of dimension-six operators influencing $f\bar{f}V$ or four-fermion couplings is given by

$$\begin{aligned}\mathcal{L}_{\text{EFT}} \supset & \frac{f_{\phi 1}}{\Lambda^2}\mathcal{O}_{\phi 1} + \frac{f_{BW}}{\Lambda^2}\mathcal{O}_{BW} + \frac{f_{LLLL}}{\Lambda^2}\mathcal{O}_{LLLL} \\ & + \frac{f_{\phi Q}^{(1)}}{\Lambda^2}\mathcal{O}_{\phi Q}^{(1)} + \frac{f_{\phi d}^{(1)}}{\Lambda^2}\mathcal{O}_{\phi d}^{(1)} + \frac{f_{\phi u}^{(1)}}{\Lambda^2}\mathcal{O}_{\phi u}^{(1)} + \frac{f_{\phi e}^{(1)}}{\Lambda^2}\mathcal{O}_{\phi e}^{(1)} + \frac{f_{\phi Q}^{(3)}}{\Lambda^2}\mathcal{O}_{\phi Q}^{(3)} \,. \end{aligned} \tag{29}$$

The couplings of the electroweak gauge bosons to fermions are well measured at LEP, the Tevatron and at the LHC, forming the set of so-called electroweak precision data on Z-pole and W-observables. At LEP, they were measured in the processes

$$e^+e^- \to Z/\gamma \to f\bar{f} \quad \text{and} \quad e^+e^- \to W^+W^- \to 4f \,. \tag{30}$$

We depict the Feynman diagrams relevant for the Z-pole observables in the SM and the contributions from dimension-six operators in Fig. 6. They probe the couplings of the Z boson to fermions as well as the two-point functions of the Z boson and the photon. For the properties of the W boson, the precision of the measurements at the LHC is already at or beyond the level of the LEP and Tevatron measurements. In the following, we will just briefly list the set of electroweak precision observables and discuss their potential for constraining the operators in our basis.

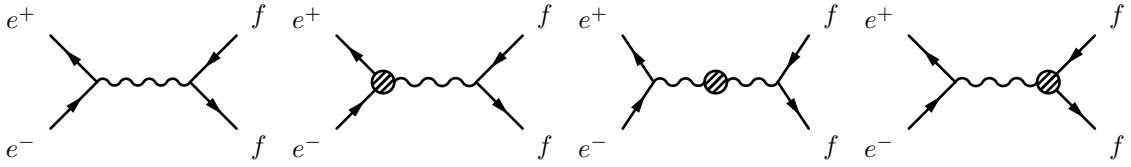

Figure 6: Feynman diagrams relevant for electroweak precision Z-pole observables in the SM (left) and contributions from dimension-six operators.

We include the Z-pole observables

$$\Big\{\Gamma_Z,\, \sigma_h^0,\, \mathcal{A}_l(\tau^{\text{pol}}),\, R_l^0,\, \mathcal{A}_l(\text{SLD}),\, A_{\text{FB}}^{0,l},\, R_c^0,\, R_b^0,\, \mathcal{A}_c,\, \mathcal{A}_b,\, A_{\text{FB}}^{0,c},\, A_{\text{FB}}^{0,b}(\text{SLD/LEP-I})\Big\} \,. \tag{31}$$

with measurements and correlations taken from Ref [53]. See Tab. 5 for explanations. Furthermore, we also include the W-observables

$$\Big\{m_W,\, \Gamma_W,\, \text{BR}(W \to l\nu)\Big\} \,, \tag{32}$$

with values taken from Ref. [54].

Due to their high precision, these observables provide strong constraints on dimension-six operators. For the inclusion of electroweak precision data in our global fit performed in Chapter 3, we follow the approach described in Ref. [46]. We use the SM predictions for above observables given in Ref. [55]. For the SM prediction of the W-mass this includes the full one- and two-loop EW and two-loop QCD corrections of $\mathcal{O}(\alpha\alpha_s)$ as well as some 3-loop contributions. The parametrization of the effects of our dimension-6 operators can be found in Ref. [46], where we limit ourselves to linear contributions from the higher-dimensional operators considered in our fit, i. e. we only take into account contributions up to $1/\Lambda$. As the typical energy scale of electroweak precision data is around m_Z, this approximation is justified as long as the dimension-6 corrections are small, i. e. $fm_Z^2/\Lambda^2 \ll 1$.

observable	definition	explanation
Γ_Z		Z boson total decay width
σ_h^0		Z boson production cross section
R_l^0	$\sigma_{\rm had}/\sigma_{ll}$	ratio of partial decay width w.r.t. hadronic decays
R_q^0	$\sigma_{q\bar{q}}/\sigma_{\rm had}$	
$A_{\rm FB}$	$(N_F - N_B)/(N_F + N_B)$	forward-backward asymmetries
$\mathcal{A}_f$	$2\,(g_{Vf}/g_{Af})/[1 + g_{Vf}/g_{Af}]$	asymmetries of left- and right-handed couplings

Table 5: Explanation of the Z-pole observables given in Eq. (31).

As a reference for the approximate size of the constraints on the Wilson coefficients of the dimension-six operators due to electroweak precision data, we quote individual limits of the standard analyses of the kind

$$\frac{\Lambda}{\sqrt{|f|}} \gtrsim 4 \ldots 10 \text{ TeV} \qquad \text{(electroweak precision data [55])}. \tag{33}$$

Comparing these limits with the expected sensitivity of the global LHC analysis from Eq. (28), we find that the reach is significantly larger in the fermionic Higgs-gauge sector. Therefore, naively it might seem that it is not necessary to combine the set of operators of the Higgs gauge sector with operators constrained by electroweak precision data in a global fit. However, we will see in Section 4 that the fermionic Higgs-gauge operators nevertheless lead to non-negligible effects at the LHC.

1.6 The Δ-framework

An arguably even simpler description of deviations from the SM in Higgs physics than effective field theory is given by the κ-framework [56–58], or the closely related Δ-framework which describes new physics effects by their influence on SM Higgs couplings. The framework relates the measured couplings of the Higgs boson to a particle x, g_x, to their SM values $g_x^{\rm SM}$ via

$$g_x = \kappa_x \, g_x^{\rm SM} = (1 + \Delta_x) \, g_x^{\rm SM} \, . \tag{34}$$

We recover the SM values for $\kappa_x = 1$ or, equivalently, $\Delta = 0$.

The simplicity of the κ/Δ-framework comes with drawbacks. As this approach is not based on any symmetries, there is no general convention for whether or not to include terms with non-SM-like Lorentz structures in the Lagrangian. As a result, Lagrangians in the Δ-framework might break gauge invariance, depending on the terms included. Furthermore, if we stick to SM-like coupling structures exclusively, we can only describe modifications of total rates, while we cannot model the effects of new physics on the kinematics as we will see, for instance, in Section 4. Finally, since the Δ-framework describes modifications of Higgs couplings only, it cannot be used to combine Higgs measurements with other precision measurements.

2 Global Fits

In the last Chapter 1, we have introduced effective field theory as a theoretically sound framework to describe new physics effects in a global and (almost) model-independent way. The next challenge that we need to tackle is to find the set of Wilson coefficients of the dimension-six operators in our basis that fit the experimental observations in the best way. More generally, we are facing the following problem: On the one hand we have a model which provides predictions for physical observables in terms of a set of free parameters. On the other hand we have a set of experimental data. Finding the configuration of model parameters that describes the data in an optimal way may seem like a straight forward task. However, it is complicated by the fact that no measurement is perfect. Any data set will suffer from uncertainties, the shape of which depend on their sources. Statistical, systematic and theoretical uncertainties lead to different probability distributions of the experimentally observed quantities or their predictions. Moreover, observables often depend on secondary measurements in control regions leading to correlations between the uncertainties of different measurements (sorry - actually we will not be talking about correlations at all, because that section of my thesis was too rough to be printed here). Taking all of the above effects into account, finding the optimal parameter values of a theory prediction to describe a given data set is the aim of a global fit.

Fitting is a two step process: First, we need to define a measure for the goodness of a parameter configuration, i. e. we need to define a quantity whose value defines the (relative) quality of a fit. Second, we need to maximize (or minimize) that quantity.

In the following, we will present the SFitter framework for performing global fits, which is used for the global analyses of the Higgs-gauge sector in the rest of these lectures. We will first discuss some basics of statistics and introduce the likelihood as a measure of the quality of a fit in Section 2.1. In Section 2.2 we will discuss the most commonly used algorithms for scanning the model parameter space and finding the parameter configuration that maximizes the likelihood. Finally, in Section 2.3, we will introduce the toy Monte Carlo method as an alternative concept to obtain best-fit points and confidence intervals in a global fit. We will closely follow the approaches of Refs. [54, 59–62].

2.1 Likelihood

In order to find a model parameter configuration that suits experimental observables in the best way, we first need to define a measure for the quality of a fit. We will now see that the likelihood is the most powerful measure of goodness of fit and demonstrate how to construct and combine likelihood functions in practice. In the next Section 2.2, we will then discuss how to optimize this measure to examine the best-fit points of our model.

When we repeatedly perform the same experiment, we expect to see different outcomes each time. Our expectation of the distribution of those different outcomes is encoded in a *probability density function* f. Integrating it, we can determine the probability P for the measured value of x to be within the interval $[x_{\min}, x_{\max}]$

$$\int_{x_{\min}}^{x_{\max}} f(x)\,\mathrm{d}x = P\,. \tag{35}$$

The probability density function (pdf) reflects our expectation of the distribution of the observable x in terms of model parameters α that we have suppressed in the above equation. In general, we should write the pdf as $f(x|\alpha)$, i. e. the probability density of x given α. To clearly separate between measured quantities and the parameters of our description, we will use Latin letters for measurements and Greek letters for model parameters in the following. Our *model* is defined as the totality of the predictions encoded by the parameters α and the assumption of the form of the pdf. The importance of the latter should not be underestimated: A global fit does not only depend on the theoretical modelling of observables, but is also influenced by our premises on the distribution of the data. We refer to a specific representation of a model for fixed parameters α as a *hypothesis* H. For the case of an effective

field theory description, the parameters α correspond to the Wilson coefficients f_i of the considered dimension-six operators. The complete model is given by the effective description of the expectation values of the experimental observables as well as the assumptions that we make for the form of the pdfs. Typical choices for the form of the pdf are a Poissonian, Gaussian or flat shape:

1. **Poisson - statistical uncertainties**
   The Poisson distribution describes the *statistical* uncertainty intrinsic to each measurement, i. e. the probability to observe d events when expecting ν_d events. It is the limit of the multinomial distribution for a small probability p, a large number of tries N and a finite number of expected events $\nu_d = N\,p$. The probability density function for the Poisson distribution is given by

$$f_{\text{Pois}}(d|\nu_d) = \frac{(\nu_d)^d}{d!}\, e^{-\nu_d}\ . \tag{36}$$

   Its variance is $\sigma_d^2 = \nu_d$. As the significance of LHC measurements is typically given in terms of the number of signal s and background b events as $s/\sqrt{b}$, the statistical significance increases with the luminosity $\mathcal{L}$ as $\sqrt{\mathcal{L}}$.

2. **Gauss - systematic uncertainties**
   In the limit of large event numbers d and ν_d, the Poisson distribution in Eq. (36) turns into a Gaussian distribution

$$f_{\text{Gauss}}(d|\nu_d) = \frac{1}{\sqrt{2\pi}\sigma_d} \exp\left(-\frac{(d-\nu_d)^2}{2\sigma_d^2}\right)\ . \tag{37}$$

   In addition to statistical uncertainties, LHC observables are also subject to uncertainties arising from external inputs, related to the apparatus used or assumptions made by the experimenter. Those *systematic* uncertainties include uncertainties on the luminosity, on photon reconstruction efficiency or the jet energy scale. Since these uncertainties are usually extracted from large data sets, we will expected them to follow a Gaussian distribution. In principle, however, systematic uncertainties could follow any distribution and the assumption of a Gaussian distribution is only an approximation.

3. **Flat - theoretical uncertainties**
   Flat uncertainty distributions are used for situations in which any outcome of a measurement within a specific range σ_d around a central value ν_d is equally probable and we do not expect the probability distribution to have any tails, $d \in [\nu_d - \sigma_d,\, \nu_d + \sigma_d]$. While this typically does not apply to experimental uncertainties, it can be relevant for *theoretical* uncertainties on the signal prediction, e. g. scale uncertainties. Scale uncertainties are usually estimated by varying the central scale μ by a factor 2. The spread between the predicted number of signal events obtained using the scales $\mu/2$ and 2μ defines the width $2\sigma_d$ which in this framework has no statistical interpretation. Within the range spanned by the two scale variations $[\nu_d^{\min},\, \nu_d^{\max}]$ we do no have a reason to favor any of the theoretical predictions and we make the conservative approximation that they are all equally probable. Beyond the boundaries set by $\mu/2$ and 2μ, we do not expect our theoretical prediction to be valid at all. Hence, we do not want any tails for the probability distribution. This behavior is represented in the probability density function for flat uncertainties by a box shape

$$f_{\text{Flat}}(\nu_d|\nu_d^{\min},\, \nu_d^{\max}) = \frac{1}{2\sigma_d}\Theta\left(\nu_d - \nu_d^{\min}\right)\,\Theta\left(\nu_d^{\max} - \nu_d\right)\ , \qquad \sigma_d = \left(\nu_d^{\max} - \nu_d^{\min}\right), \tag{38}$$

   using the Heaviside function Θ. Notice that Eq. (38) describe the probability density function for the prediction ν_d and not for the measurement d. Nevertheless, in SFitter, we often apply theory uncertainties to the measured signal instead of the theory prediction. This is an approximation made for convenience only.

The interpretation of the probability density functions $f(x|\alpha)$ as a function of α with fixed x is called the *likelihood* $L(\alpha) = L(x|\alpha) = f(x|\alpha)$. It is important to notice that the likelihood cannot be

interpreted as a probability in terms of α. Specifically, it is not normalized and it does not correspond to the probability of a model parameter configuration given the data. For practical reasons, instead of handling the likelihood directly, it is common to work with negative log-likelihood $-2\log L(\alpha)$. This has the advantage that a product of likelihood functions becomes a simple sum of log-likelihood functions.

Likelihood ratios and statistical tests

Our aim for this section was to find a measure that quantifies the level of agreement between the data and a hypothesis. Let us now come back to this problem in a realistic environment: In practice, instead of a single observable we are usually confronted with a set of measurements $\mathcal{D} = \{x_1, ..., x_n\}$ that we will refer to as the data. Our theoretical description of the data is characterized by the parameters $\alpha = \{\alpha_1, ..., \alpha_k\}$ which we want to fit, i. e. for which we want to find the optimal configuration. A measure for the goodness of fit should map the data to a single real number. Such function is called a *test statistic* $T(\mathcal{D}) \to \mathbb{R}$. The likelihood function is one example of a test statistic. It has been shown by Neyman-Pearson that for a hypothesis test of the hypothesis H_1 against the zero hypothesis H_0 the test statistic leading to the most powerful test is the likelihood ratio [63, 64]

$$T_{\text{NP}} = \frac{L(\mathcal{D}|H_1)}{L(\mathcal{D}|H_0)}\,. \tag{39}$$

In a way, our problem of trying to obtain an optimal parameter configuration for describing a given data set is closely related to the problem of hypothesis testing. However, instead of comparing two hypothesis explicitly, we want to quantify the level of agreement between the data and a hypothesis without an explicit reference to an alternative. There exists no equivalent of the Neyman-Pearson lemma in Eq. (39) for models with several free parameters. We can, nevertheless, generalize its idea and construct the profile likelihood ratio. Before we discuss this test statistic, we should first introduce the concept of nuisance parameters.

In many applications, the set of model parameters α consists not only of the parameters of interest, i. e. the parameters that we ultimately want to fit, but also additional parameters which are relevant for an accurate description of the model without being of intrinsic interest. We will refer to those parameters as *nuisance parameters*, $\alpha = \{\alpha_{\text{poi}}, \alpha_{\text{nui}}\}$. Let us explain this concept using an explicit example relevant for LHC physics: For LHC measurements, the quantities that we measure, i. e. our data d, will always contain a combination of the signal s that we are interested in and an indistinguishable background b, $d = s+b$. The predicted number of background events ν_b will hence enter our extraction of the signal as a nuisance parameter. One way of dealing with these additional parameter in our likelihood function, is to maximize the likelihood with respect to the nuisance parameters $\sup_{\alpha_{\text{nui}}} L(\alpha)$. This process is called *profiling* and we will write the corresponding profile likelihood as $L_p(\alpha) = L(\alpha, \hat{\hat{\alpha}}_{\text{nui}})$, where the double-hat notation denotes the profiled values of the nuisance parameters.

As a test statistic which is particularly useful for limit setting, we can now introduce the profile likelihood ratio

$$T_p(\alpha) = \frac{L(\alpha, \hat{\hat{\alpha}}_{\text{nui}})}{L(\alpha_{\text{best}})} = \frac{L_p(\alpha)}{L(\alpha_{\text{best}})}\,, \tag{40}$$

i. e. the ratio of the profile likelihood and the likelihood at the best-fit point. Comparing the definition of the profile likelihood ratio to the ratio used in the Neyman-Pearson lemma in Eq. (39), we find that the parameter configuration maximizing the likelihood plays the role of the zero hypothesis. The advantage of the profile likelihood ratio is that for large data sample sizes, the distribution of $-2\log T_p(\alpha)$ follows a χ^2 distribution with the number of degrees of freedom being given by the number of parameters α [65, 66]. Using the profile likelihood as a test statistic therefore allows us to make use of the known properties of the χ^2 distribution for limit setting. For the application of fitting Wilson coefficients of dimension-six operators, for instance, we can set limits on a Wilson coefficients f_x by treating all other coefficients as nuisance parameters and profiling over them. We can then treat $-2\log T_p(f_x)$ with a single free Wilson coefficient f_x as a χ^2 distribution with one degree of freedom

and obtain the 2σ limits by evaluating $\Delta\chi^2 = 4$.

In order to motivate the concept of profiling, let us introduce the p-value, a common measure of the significance of the data and a hypothesis $H(\alpha)$. It is defined as the probability of finding the test statistic T in the region of equal or greater incompatibility with the hypothesis than the level of compatibility observed with the actual data, characterized by T_{obs}. Assuming a large value of the test statistics corresponds to poor agreement of data and hypothesis (as is the case for the log-likelihood), the p-value is given by

$$p = \int_{T_{\text{obs}}}^{\infty} L(T|H)\, \mathrm{d}T = \int_{T_{\text{obs}}}^{\infty} f(T|\alpha)\, \mathrm{d}T = P(T \geq T_{\text{obs}}|\alpha)\,. \tag{41}$$

A small p-value signals a small probability of finding a test statistic as large as or greater than the observed value T_{obs}. The concept of p-values is used to exclude null hypotheses. Let us now study the influence of nuisance parameters on the p-value. In order to be conservative, i. e. in order not to exclude a null hypothesis based on its small p-value, we should maximize the p-value of the hypothesis that we are testing with respect to variations of the nuisance parameters. This corresponds to maximizing the integrand in Eq. (41), the likelihood. Profiling over the nuisance parameters is hence the most conservative approach we can take when working with p-values.

In particle physics, it is common to translate the p-value in Eq. (41) into an equivalent significance Z defined such that a Gaussian distributed variable found Z standard deviation above its mean has an upper-tail probability of p, i. e.

$$Z = \Phi^{-1}(1 - p)\,, \tag{42}$$

where Φ denotes the inverse of the cumulative distribution of the standard Gaussian. A significance $Z = 5$ is typically used in particle physics to claim a discovery. This corresponds to a p-value of $p = 2.9 \times 10^{-7}$.

Combination of likelihood functions

We have found above that the likelihood is the most powerful measure for the goodness of a fit. In Eqs. (36), (37) and (38), we have discussed the likelihood functions for statistical, systematic or theoretical uncertainties respectively for a single measurement d and model parameters $\{\nu_d, \sigma_d\}$. In the real world, however, we usually have to construct a combined likelihood function for several measurements which are subject to various types of uncertainties. When f are the probability density functions of n independent and identically distributed measurements $\mathbf{x}$ in a data set $\mathcal{D}$, then the combined likelihood is given by

$$L(\alpha) = L(\mathcal{D}|\alpha) = \prod_{i=1}^{n} f(x_i|\alpha)\,. \tag{43}$$

In practice, the measurements whose likelihood we need to combine often depend on each other. As an example of dependent measurements, let us come back to the discussion of backgrounds as a nuisance parameter, see the paragraph below Eq. (39). Often, we do not have access to a signal measurement s directly, but we need to extract it from a measurement d that contains an indistinguishable background b, $s = d - b$. The number of background events b is often measured in a control region and enters our signal determination as a nuisance parameter. The combined likelihood is a convolution of the measurements in the signal and control regions

$$L_{\text{Pois}}(\nu_s, \nu_b) = L_{\text{Pois}}(d|\nu_s, \nu_b) L_{\text{Pois}}(b_{\text{CR}}|\nu_{b,\text{CR}}) = \frac{(\nu_s + \nu_b)^d}{d!}\, e^{-(\nu_s+\nu_b)}\, \frac{(\tau\nu_b)^{b_{\text{CR}}}}{b_{\text{CR}}!}\, e^{-\tau\nu_b}\,, \tag{44}$$

where $\tau = \nu_{b,\text{CR}}/\nu_b$ is a scale factor. It has been inserted to account for the fact that the expected number of background events in the control region often differs from that in the signal region, as one tries to reduce the statistical uncertainty by to extracting the number of background events in a larger

region. The estimated number of background events ν_b is a typical example of a nuisance parameter. It is irrelevant for our modelling of the signal which we ultimately want to constrain, but enters its extraction from a measurement. As discussed in the paragraph below Eq. (39), we deal with nuisance parameters by profiling over them, leading to the combined likelihood

$$L_{\text{Pois}}(\nu_s) = \max_{\nu_b^*} \frac{(\nu_s + \nu_b^*)^d}{d!} e^{-(\nu_s+\nu_b^*)} \frac{(\tau\nu_b^*)^{b_{\text{CR}}}}{b_{\text{CR}}!} e^{-\tau\nu_b^*} . \tag{45}$$

In general, the we cannot perform the profiling analytically. While there exist analytical solutions for the combination of likelihood functions based on flat and Gaussian probability density functions, the likelihood combination for Poissonian distributions has to be performed numerically. In SFitter, we combine of two Poisson likelihoods using the approximate formula [58]

$$\frac{1}{\log L_{\text{comb}}} \approx \frac{1}{\log L_{\text{Pois},1}} + \frac{1}{\log L_{\text{Pois},2}} , \tag{46}$$

which becomes exact in the Gaussian limit.

2.2 Fitting techniques

With the (log-)likelihood, we have defined a measure for comparing the quality of the agreement of a parameter configuration with a given data set. The challenge for fitting tools like SFitter is now to find best fit parameter configuration, i. e. to maximize the likelihood or to minimize the log-likelihood or χ^2. In the following, we will explain several techniques for likelihood maximization and discuss their strengths and weaknesses. Starting from a simple grid fit, we will discuss more complex fitting algorithms like Migrad which is using gradient descent and Markov Chain Monte Carlos. In the next Section 2.3, we will present toy Monte Carlos as an alternative approach to obtain best-fit points and confidence limits.

All of the above mentioned fitting techniques come with advantages and drawbacks for specific applications. Best-fit points and limits in a multidimensional parameter space can be obtained with toy Monte Carlos in a computationally inexpensive way. For correlations and scans of complex likelihood functions with multiple minima, however, a Markov Chain fit is potentially more suitable.

Grid

Arguably the most intuitive fitting technique for a model with n free parameters is to build an n-dimensional grid of the parameter space and find the point in the grid with the largest likelihood. Clearly, this is not only a very simple approach, but also a very inefficient one, since the density of points tested in a grid is completely unrelated to the likelihood. The computation time grows as x^n with x being the number of points tested per parameter which makes it intractable for a large number of fitting parameters.

Migrad

Migrad [67, 68] is a minimization algorithm based on gradient descent. Starting from a point α_k in parameter space, it chooses the next point α_{k+1} by moving along the gradient of the function $l(\alpha)$ that we want to minimize (in our case the log-likelihood) using a predefined step size s_k

$$\alpha_{k+1} = \alpha_k - s_k \nabla l(\alpha). \tag{47}$$

Following the gradient, the algorithm will lead eventually end up in a local minimum of the function $l(\alpha)$. The effective step size $\alpha_{k+1} - \alpha_k$ will become smaller and the evaluation of the log-likelihood more detailed close to the minimum as the gradient tends to zero in the vicinity of the minimum. In contrast to a grid fit, the test point density in a Migrad fit will therefore be larger close to the best fit point.

The method of steepest descent that we have discussed so far only specifies the direction of the next step, but not its length s_k. For correlated parameters this methods will converge very slowly. To overcome this issue, the Newton method uses the inverse of the Hessian matrix as the variable step size

$$\alpha_{k+1} = \alpha_k - H_l(\alpha)^{-1} \nabla l(\alpha) = \alpha_k - \left(\frac{\partial l(\alpha)}{\partial \alpha_i \partial \alpha_j} \right)^{-1} \nabla l(\alpha) \,. \tag{48}$$

The algorithm is effectively approximating $l(\alpha)$ as a quadratic function and the step suggested by it is the step to the minimum of this quadratic approximation. Larger step sizes will therefore be proposed further away from the minimum. While each step in the minimization is computationally very expensive in the Newton method as it includes calculating the matrix of second derivatives and the inversion of such matrix, the convergence of the algorithm is very efficient. If $l(\alpha)$ is in fact a quadratic function, the algorithm converges in one step. MIGRAD is using a variant of this method.

Markov Chains

A Markov chain is a sequence of points in parameter space for which the conditional probability distribution of choosing the next point α_{k+1} in parameter space depends only on the present point α_k and not on any previous part of the chain [69]. Markov chains are a well-established tool for the maximization of likelihoods with complex functional dependencies, e. g. with multiple minima, or a large number of parameters [70, 71].

In practice, the probability distribution used as a criterion for the acceptance of new points is the likelihood. We randomly choose a point α_{test} in parameter space and compare its likelihood to the likelihood of the current point of the Markov Chain. If the likelihood of the test point is larger than that of the current point, we directly accept it as the next element of the chain. Otherwise, we test if the likelihood of the point fulfills the condition

$$\frac{L(\alpha_{\text{test}})}{L(\alpha_k)} \geq r \tag{49}$$

with r being a random number in the range $[0, 1]$ and accept the point if the condition is fulfilled [72,73]. The algorithm will move towards the best fit point and explore the area close to it. In the ideal case Markov Chains scale only linearly with the number of input parameters, allowing for fits of a multidimensional parameter space.

To increase the performance of the Markov chain, we have two handles: We can either make the generation of test points more efficient or we can modify the probability of accepting points as described by Eq. (49). Taking the first of the two approaches, we can choose our test points from a random distribution around the current element of the chain α instead of choosing αtest completely randomly. As the likelihood is usually a continuous function of the fit parameters, points close to an element with a (large) likelihood can be expected to have a similarly large likelihood. We can therefore choose test points from e. g. a Breit-Wigner or a Gaussian distribution around the current point.

Alternatively, we can also increase the efficiency of the Markov Chain by modifying the acceptance criterion for new chain elements. A common approach coined *cooling* reduces the probability of a point with a smaller likelihood to be accepted as the next element of the chain depending on its position in the chain [58,74]. For this, we divide the Markov chain into 100 segments numbered with $j = 1 \cdots 100$ and replace the right hand side of Eq. (49) by

$$\frac{L(\alpha_{\text{test}})}{L(\alpha_k)} \geq r^{\frac{100}{j \cdot c}} \,, \tag{50}$$

with a cooling factor $c \sim 10$. At an early stage of the Makov chain, i. e. for small values of j, when our aim is to perform a rough scan to make sure that we will find multiple minima, the right hand side is close to zero and almost all points are accepted. With increasing j the threshold for a test point to be

accepted as the next element of the chain is raised. Therefore, the Markov chain will focus on finding better estimates of the best fit point during its the later stages.

Markov chains are useful for broader scans of the parameter space and for finding multiple minima. If one is only interested in finding the best-fit point in parameter space, there are more efficient algorithms like MIGRAD which are better suited for such problems. The breadth of the scanned parameter space makes Markov Chains particularly useful for examining correlations.

2.3 Toy Monte Carlos

So far, the algorithms discussed to find the best fit points of a fit where based on the minimization of the log-likelihood. Given a set of measurements, we were trying to find the point in parameter space that best describes the data. The *toy Monte Carlo method* is a different way of obtaining best fit points and confidence limits. It is also know under the name of *Monte Carlo (replica) method* in the PDF fitting community [75–77]. The idea of the toy Monte Carlo method is to create large number of artificial data sets, based on the experimental central values, uncertainties, and correlation associated with each measurement. For each pseudo measurement, we shift the data within their uncertainties, respecting the different nature of different sources of uncertainties (flat, Poissonian, Gaussian), and their correlations. The resulting set of artificial replicas can then be analyzed using textbook methods. We create a replica of measurement i with experimental value x_i^{exp} using

$$\begin{aligned} x_i^{\text{toy}} &= x_i^{\text{exp}} + \Delta^{\text{shift}} + \text{sign}(\Delta^{\text{shift}})\Delta^{\text{flat}} \\ \Delta^{\text{shift}} &= \Delta^{\text{Gaus}} + \Delta^{\text{Pois}} + \Delta^{\text{syst}} \end{aligned} \tag{51}$$

where

$$\Delta^{\text{Gaus}} = r^{\text{Gaus}} \sqrt{\sum_j (\sigma_j^{\text{Gaus}})^2} \qquad \Delta^{\text{Pois}} = \frac{r^{\text{Pois}}(\tau x_i^{\text{toy}})}{\tau} - x_i^{\text{toy}} \tag{52}$$

$$\Delta^{\text{syst}} = \sum_{j=1}^{N_{\text{syst}}} r_j^{\text{syst}} \sigma_j^{\text{syst}} \qquad \Delta^{\text{flat}} = \sum_{j=1}^{N_{\text{flat}}} \sigma_j^{\text{flat}} \tag{53}$$

r^{Gaus}, $r_j^{\text{syst}} \in \text{Gauss}(0, 1)$ are random numbers drawn from a uniform distrbution. $r^{\text{Pois}}(x)$ is a random integer drawn from a Poissonian distribution with mean x and τ denotes the factor between the size of the signal and control regions.

For each of those smeared pseudo data sets we calculate the best-fit point using an appropriate fitter (e.g. Minuit). We then create one-dimensional histograms of the best-fit points of the toy Monte Carlo data in terms of the model parameters, implicitly profiling over the other model parameters. For large data sets, these histograms will follow a Gaussian distribution. We deduce the mean and confidence limits of the model parameters using textbook methods.

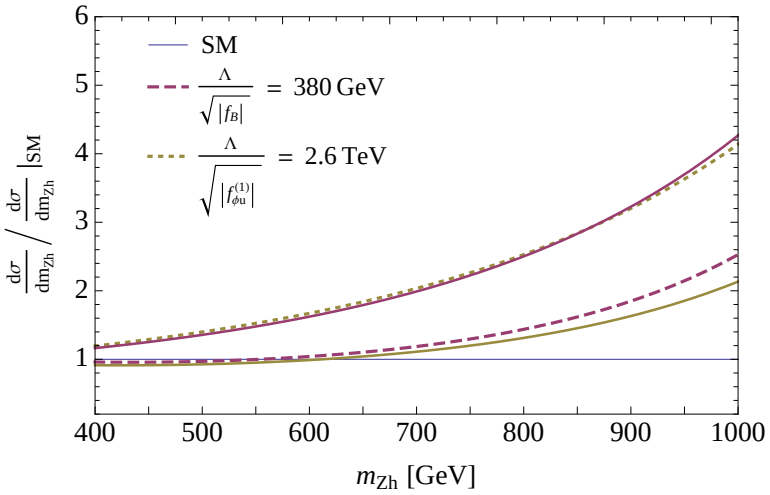

Figure 7: Invariant mass distribution m_{Zh} normalized to the Standard Model. The dashed lines correspond to $\Lambda/\sqrt{|f_B|} = 380$ GeV and $\Lambda/\sqrt{|f_{\phi u}^{(1)}|} = 2.6$ TeV with $f_x > 0$, while the solid lines correspond to the negative values of the Wilson coefficients with the same magnitude. Figure taken from Ref. [84].

3 Global fits for LHC Run II

See corresponding slides

We start from the effective Lagrangian defined in Refs [37, 38, 47]

$$\begin{aligned}\mathcal{L}_{\text{eff, 1}} = &-\frac{\alpha_s}{8\pi}\frac{f_{GG}}{\Lambda^2}\mathcal{O}_{GG} + \frac{f_{WW}}{\Lambda^2}\mathcal{O}_{WW} + \frac{f_{BB}}{\Lambda^2}\mathcal{O}_{BB} + \frac{f_W}{\Lambda^2}\mathcal{O}_W + \frac{f_B}{\Lambda^2}\mathcal{O}_B \\ &+ \frac{f_{\phi 2}}{\Lambda^2}\mathcal{O}_{\phi 2} + \frac{f_{WWW}}{\Lambda^2}\mathcal{O}_{WWW} \\ &+ \frac{f_\tau m_\tau}{v\Lambda^2}\mathcal{O}_{e\phi,33} + \frac{f_b m_b}{v\Lambda^2}\mathcal{O}_{d\phi,33} + \frac{f_t m_t}{v\Lambda^2}\mathcal{O}_{u\phi,33} + \text{invisible decays}\,, \end{aligned} \tag{54}$$

using the operator definitions in Eqs. (8)–11.

In addition, we explicitly include the operators with tree-level contributions to electroweak precision observables, as we know that at the level of 13 TeV data the corresponding operators should not be neglected [45, 46, 78–83]

$$\begin{aligned}\mathcal{L}_{\text{eff,2}} = &\frac{f_{\phi Q}^{(1)}}{\Lambda^2}\mathcal{O}_{\phi Q}^{(1)} + \frac{f_{\phi d}^{(1)}}{\Lambda^2}\mathcal{O}_{\phi d}^{(1)} + \frac{f_{\phi u}^{(1)}}{\Lambda^2}\mathcal{O}_{\phi u}^{(1)} + \frac{f_{\phi e}^{(1)}}{\Lambda^2}\mathcal{O}_{\phi e}^{(1)} + \frac{f_{\phi Q}^{(3)}}{\Lambda^2}\mathcal{O}_{\phi Q}^{(3)} \\ &+ \frac{f_{\phi 1}}{\Lambda^2}\mathcal{O}_{\phi 1} + \frac{f_{BW}}{\Lambda^2}\mathcal{O}_{BW} + \frac{f_{LLLL}}{\Lambda^2}\mathcal{O}_{LLLL}\,. \end{aligned} \tag{55}$$

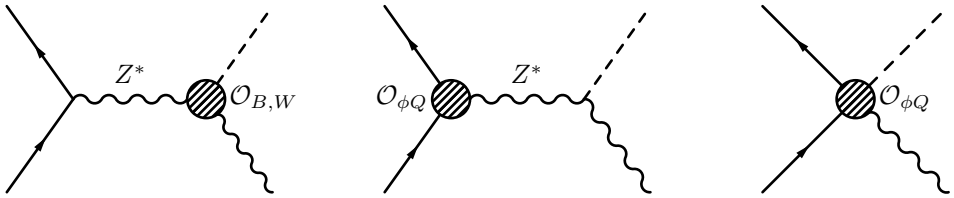

Figure 8: Dimension-6 contribution to Zh production. We show sample diagrams for the usual bosonic corrections, the small fermionic corrections from a 3-point vertex, and the large fermionic corrections from a 4-point interaction.

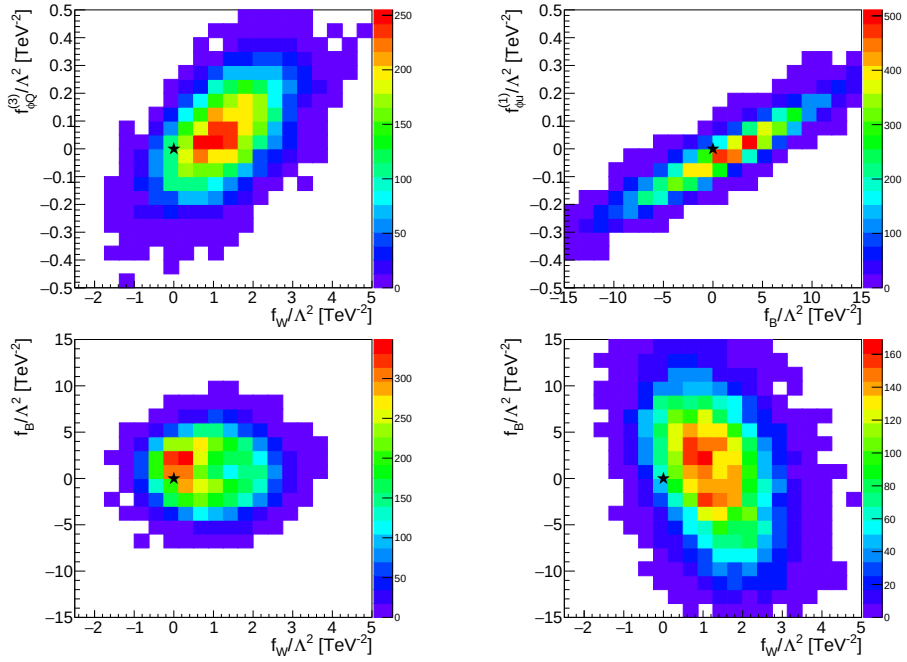

Figure 9: Correlations between the fermionic and bosonic operators (top row), and between the usual bosonic operators (bottom row). For the latter we show the purely LHC results (left) and the results after including the additional fermionic operators. Figure taken from Ref. [84].

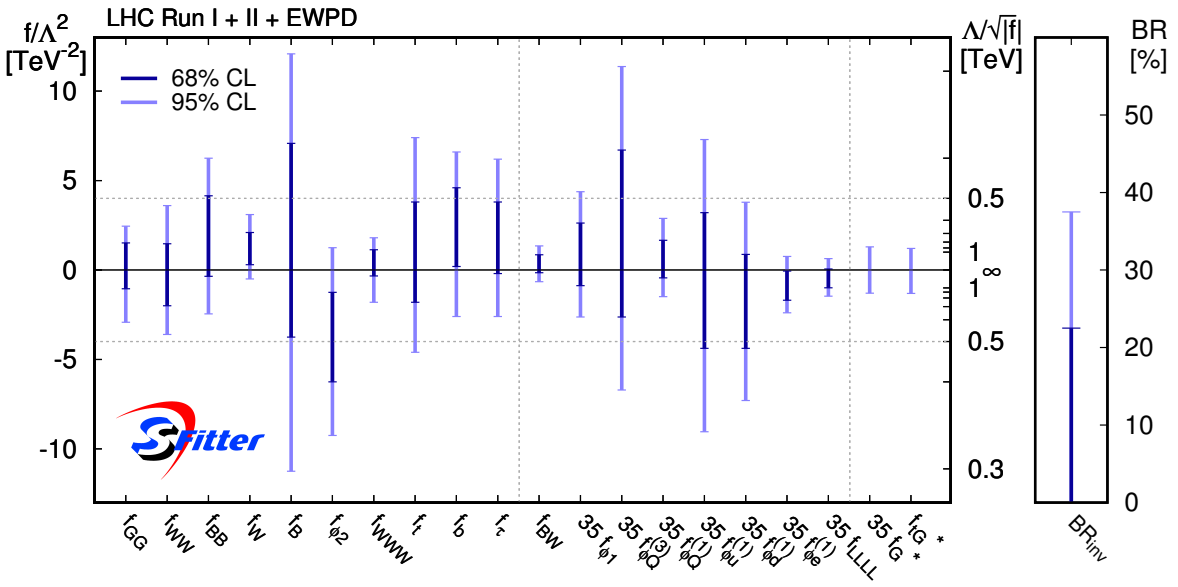

Figure 10: Allowed 68% and 95% CL ranges for individual Wilson coefficients f_x/Λ^2 from a one-dimensional profile likelihood. All results include the Run II measurements combined with electroweak precision data. We quote the best results for $\mathcal{O}_G$ [85] and $\mathcal{O}_{tG}$ [86] from non-Higgs analyses. Figure taken from Ref. [84].

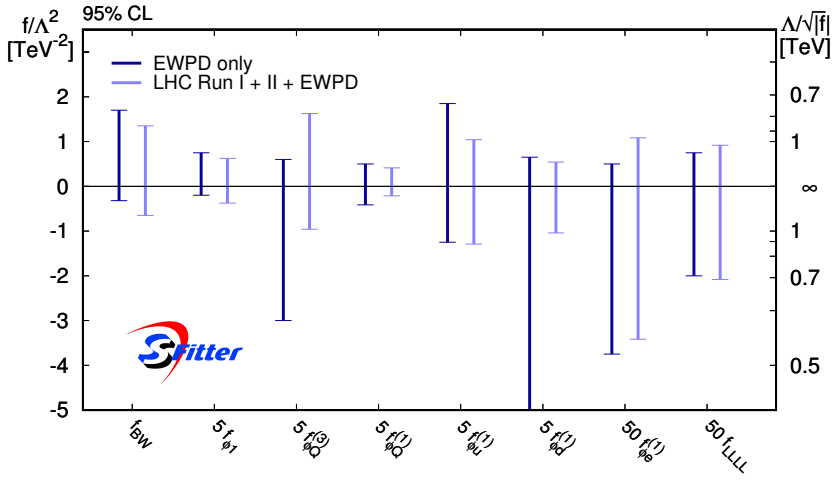

Figure 11: Allowed 95% CL ranges for the individual Wilson coefficients f_x/Λ^2 constrained in electroweak precision data, see Eq. (55), from a one-dimensional profile likelihood. We compare fits using electroweak precision data as inputs only with a combined fit including LHC Run I and Run II measurements.

4 Global fits for a 27 TeV pp collider

See corresponding slides

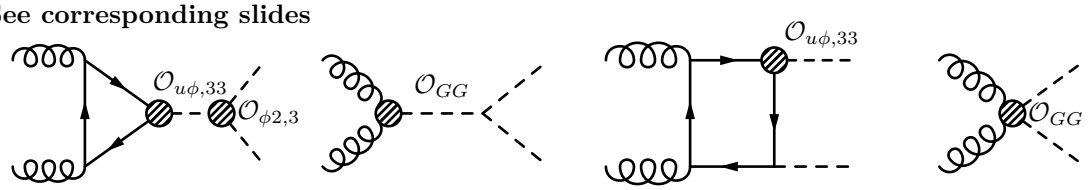

Figure 12: Feynman diagrams of the dominant modes for di-Higgs production including contributions from the dimension-six operators in the effective Lagrangian in Eq. **??**.

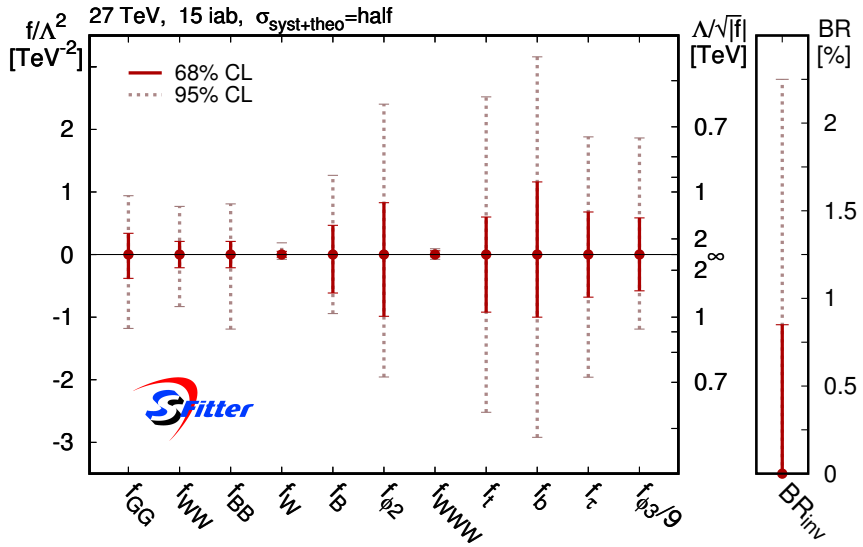

Figure 13: Result from the global Higgs analysis in terms of dimension-6 operators, complementing the high-luminosity and improved-error scenario of Fig. ?? with results for 95% CL or two standard deviations. Figure taken from Ref. [?].

A EFT basis

In Section 1.3, we have explicitly listed the operators relevant for our study of Higgs physics. Here, we want to list the remaining operators in our basis for completeness. We will only list the operators including bosonic fields and refer to Table 1 of Ref. [87] for a complete list of four-fermion operators.

There are six bosonic CP-violating operators

$$\begin{aligned}
&\mathcal{O}_{G\tilde{G}} = \phi^\dagger\phi\, G^a_{\mu\nu}\tilde{G}^{a\mu\nu} && \mathcal{O}_{B\tilde{B}} = -\frac{g'^2}{4}\phi^\dagger B_{\mu\nu}\tilde{B}^{\mu\nu}\phi && \mathcal{O}_{W\tilde{W}} = -\frac{g^2}{4}\phi^\dagger W_{\mu\nu}\tilde{W}^{\mu\nu}\phi \\
&\mathcal{O}_{B\tilde{W}} = -\frac{gg'}{4}\phi^\dagger B_{\mu\nu}\tilde{W}^{\mu\nu}\phi && \mathcal{O}_{WW\tilde{W}} = -\frac{ig^3}{8}\,\mathrm{Tr}\left(\tilde{W}_{\mu\nu}W^{\nu\rho}W^{\mu}_{\rho}\right) && \mathcal{O}_{\tilde{G}} = f_{abc}\tilde{G}^{\rho}_{a\nu}G^{\nu}_{b\lambda}G^{\lambda}_{c\rho}\,,
\end{aligned} \tag{56}$$

where we explicitly write out additional powers of the coupling strength g and g' instead of using the hatted fields as in Eq. (9) and the dual field strength tensors are defined as

$$\tilde{V}_{\mu,\nu} = \frac{1}{2}\epsilon_{\mu\nu\rho\sigma}V^{\rho\sigma}\,, \tag{57}$$

for $V = B$, W, G.
There are eight dipole operators, fermionic Higgs-gauge operators with a non SM-like Lorentz structure

$$\begin{aligned}
&\mathcal{O}_{uW} = (\bar{Q}\sigma^{\mu\nu}u_R)\tau^a\,\tilde{\phi}\,W^a_{\mu\nu} && \mathcal{O}_{uB} = (\bar{Q}\sigma^{\mu\nu}u_R)\,\tilde{\phi}\,B_{\mu\nu} && \mathcal{O}_{uG} = (\bar{Q}\sigma^{\mu\nu}T^a u_R)\,\tilde{\phi}\,G^a_{\mu\nu} \\
&\mathcal{O}_{dW} = (\bar{Q}\sigma^{\mu\nu}d_R)\tau^a\,\phi\,W^a_{\mu\nu} && \mathcal{O}_{dB} = (\bar{Q}\sigma^{\mu\nu}d_R)\,\phi\,B_{\mu\nu} && \mathcal{O}_{dG} = (\bar{Q}\sigma^{\mu\nu}T^a d_R)\,\phi\,G^a_{\mu\nu} \\
&\mathcal{O}_{\ell W} = (\bar{L}\sigma^{\mu\nu}\ell_R)\tau^a\,\phi\,W^a_{\mu\nu} && \mathcal{O}_{\ell B} = (\bar{L}\sigma^{\mu\nu}\ell_R)\,\phi\,B_{\mu\nu}\,.
\end{aligned} \tag{58}$$

References

[1] **ATLAS** Collaboration, G. Aad *et al.*, "Observation of a new particle in the search for the Standard Model Higgs boson with the ATLAS detector at the LHC," *Phys. Lett.* **B716** (2012) 1–29, arXiv:1207.7214 [hep-ex].

[2] **CMS** Collaboration, S. Chatrchyan *et al.*, "Observation of a new boson at a mass of 125 GeV with the CMS experiment at the LHC," *Phys. Lett.* **B716** (2012) 30–61, arXiv:1207.7235 [hep-ex].

[3] P. W. Higgs, "Broken Symmetries and the Masses of Gauge Bosons," *Phys. Rev. Lett.* **13** (1964) 508–509. [,160(1964)].

[4] P. W. Higgs, "Broken symmetries, massless particles and gauge fields," *Phys. Lett.* **12** (1964) 132–133.

[5] F. Englert and R. Brout, "Broken Symmetry and the Mass of Gauge Vector Mesons," *Phys. Rev. Lett.* **13** (1964) 321–323. [,157(1964)].

[6] S. Dawson, C. Englert, and T. Plehn, "Higgs Physics: It ain't over till it's over," arXiv:1808.01324 [hep-ph].

[7] C. N. Leung, S. T. Love, and S. Rao, "Low-Energy Manifestations of a New Interaction Scale: Operator Analysis," *Z. Phys.* **C31** (1986) 433.

[8] W. Buchmuller and D. Wyler, "Effective Lagrangian Analysis of New Interactions and Flavor Conservation," *Nucl. Phys.* **B268** (1986) 621–653.

[9] M. C. Gonzalez-Garcia, "Anomalous Higgs couplings," *Int. J. Mod. Phys.* **A14** (1999) 3121–3156, arXiv:hep-ph/9902321 [hep-ph].

[10] B. Grzadkowski, M. Iskrzynski, M. Misiak, and J. Rosiek, "Dimension-Six Terms in the Standard Model Lagrangian," *JHEP* **10** (2010) 085, arXiv:1008.4884 [hep-ph].

[11] G. Passarino, "NLO Inspired Effective Lagrangians for Higgs Physics," *Nucl. Phys.* **B868** (2013) 416–458, arXiv:1209.5538 [hep-ph].

[12] J. Brehmer, *New Ideas for Effective Higgs Measurements*. PhD thesis, U. Heidelberg (main), 2017. http://www.thphys.uni-heidelberg.de/~plehn/includes/theses/brehmer_d.pdf.

[13] T. Corbett, *Effective Lagrangians for Higgs physics*. PhD thesis, Stony Brook U., 2015-04-30. http://graduate.physics.sunysb.edu/announ/theses/corbett-tyler-may-2015.pdf.

[14] S. L. Glashow, "Partial Symmetries of Weak Interactions," *Nucl. Phys.* **22** (1961) 579–588.

[15] A. Salam and J. C. Ward, "Electromagnetic and weak interactions," *Phys. Lett.* **13** (1964) 168–171.

[16] S. Weinberg, "A Model of Leptons," *Phys. Rev. Lett.* **19** (1967) 1264–1266.

[17] J. Goldstone, A. Salam, and S. Weinberg, "Broken Symmetries," *Phys. Rev.* **127** (1962) 965–970.

[18] Y. Nambu, "Axial vector current conservation in weak interactions," *Phys. Rev. Lett.* **4** (1960) 380–382. [,107(1960)].

[19] J. Goldstone, "Field Theories with Superconductor Solutions," *Nuovo Cim.* **19** (1961) 154–164.

[20] **LHC Higgs Cross Section Working Group** Collaboration, D. de Florian *et al.*, "Handbook of LHC Higgs Cross Sections: 4. Deciphering the Nature of the Higgs Sector," arXiv:1610.07922 [hep-ph].

[21] R. Contino, A. Falkowski, F. Goertz, C. Grojean, and F. Riva, "On the Validity of the Effective Field Theory Approach to SM Precision Tests," *JHEP* **07** (2016) 144, arXiv:1604.06444 [hep-ph].

[22] E. Fermi, "An attempt of a theory of beta radiation. 1.," *Z. Phys.* **88** (1934) 161–177.

[23] S. Weinberg, "Phenomenological Lagrangians," *Physica* **A96** (1979) no. 1-2, 327–340.

[24] H. Georgi, *Weak Interactions and Modern Particle Theory.* 1984.

[25] J. F. Donoghue, E. Golowich, and B. R. Holstein, "Dynamics of the standard model," *Camb. Monogr. Part. Phys. Nucl. Phys. Cosmol.* **2** (1992) 1–540. [Camb. Monogr. Part. Phys. Nucl. Phys. Cosmol.35(2014)].

[26] A. De Rujula, M. B. Gavela, P. Hernandez, and E. Masso, "The Selfcouplings of vector bosons: Does LEP-1 obviate LEP-2?," *Nucl. Phys.* **B384** (1992) 3–58.

[27] K. Hagiwara, S. Ishihara, R. Szalapski, and D. Zeppenfeld, "Low-energy effects of new interactions in the electroweak boson sector," *Phys. Rev.* **D48** (1993) 2182–2203.

[28] K. Hagiwara, S. Matsumoto, and R. Szalapski, "Constraints on new physics in the electroweak bosonic sector from current data and future experiments," *Phys. Lett.* **B357** (1995) 411–418, arXiv:hep-ph/9505322 [hep-ph].

[29] K. Hagiwara, T. Hatsukano, S. Ishihara, and R. Szalapski, "Probing nonstandard bosonic interactions via W boson pair production at lepton colliders," *Nucl. Phys.* **B496** (1997) 66–102, arXiv:hep-ph/9612268 [hep-ph].

[30] T. Corbett, O. J. P. Eboli, J. Gonzalez-Fraile, and M. C. Gonzalez-Garcia, "Constraining anomalous Higgs interactions," *Phys. Rev.* **D86** (2012) 075013, arXiv:1207.1344 [hep-ph].

[31] T. Corbett, O. J. P. Eboli, J. Gonzalez-Fraile, and M. C. Gonzalez-Garcia, "Robust Determination of the Higgs Couplings: Power to the Data," *Phys. Rev.* **D87** (2013) 015022, arXiv:1211.4580 [hep-ph].

[32] J. Brehmer, F. Kling, T. Plehn, and T. M. P. Tait, "Better Higgs-CP Tests Through Information Geometry," *Phys. Rev.* **D97** (2018) no. 9, 095017, arXiv:1712.02350 [hep-ph].

[33] F. U. Bernlochner, C. Englert, C. Hays, K. Lohwasser, H. Mildner, A. Pilkington, D. D. Price, and M. Spannowsky, "Angles on CP-violation in Higgs boson interactions," *Phys. Lett.* **B790** (2019) 372–379, arXiv:1808.06577 [hep-ph].

[34] G. F. Giudice, P. Paradisi, and M. Passera, "Testing new physics with the electron g-2," *JHEP* **11** (2012) 113, arXiv:1208.6583 [hep-ph].

[35] A. Buckley, C. Englert, J. Ferrando, D. J. Miller, L. Moore, M. Russell, and C. D. White, "Global fit of top quark effective theory to data," *Phys. Rev.* **D92** (2015) no. 9, 091501, arXiv:1506.08845 [hep-ph].

[36] **CDF, D0** Collaboration, T. Aaltonen *et al.*, "Combination of CDF and D0 measurements of the W boson helicity in top quark decays," *Phys. Rev.* **D85** (2012) 071106, arXiv:1202.5272 [hep-ex].

[37] T. Corbett, O. J. P. Eboli, D. Gonçalves, J. Gonzalez-Fraile, T. Plehn, and M. Rauch, "The Higgs Legacy of the LHC Run I," *JHEP* **08** (2015) 156, arXiv:1505.05516 [hep-ph].

[38] T. Corbett, O. J. P. Eboli, D. Gonçalves, J. Gonzalez-Fraile, T. Plehn, and M. Rauch, "The Non-Linear Higgs Legacy of the LHC Run I," arXiv:1511.08188 [hep-ph].

[39] J. de Blas, O. Eberhardt, and C. Krause, "Current and Future Constraints on Higgs Couplings in the Nonlinear Effective Theory," *JHEP* **07** (2018) 048, arXiv:1803.00939 [hep-ph].

[40] M. E. Peskin and T. Takeuchi, "A New constraint on a strongly interacting Higgs sector," *Phys. Rev. Lett.* **65** (1990) 964–967.

[41] M. E. Peskin and T. Takeuchi, "Estimation of oblique electroweak corrections," *Phys. Rev.* **D46** (1992) 381–409.

[42] V. Cirigliano, J. Jenkins, and M. Gonzalez-Alonso, "Semileptonic decays of light quarks beyond the Standard Model," *Nucl. Phys.* **B830** (2010) 95–115, arXiv:0908.1754 [hep-ph].

[43] A. Falkowski, M. González-Alonso, and K. Mimouni, "Compilation of low-energy constraints on 4-fermion operators in the SMEFT," *JHEP* **08** (2017) 123, arXiv:1706.03783 [hep-ph].

[44] S. Alioli, V. Cirigliano, W. Dekens, J. de Vries, and E. Mereghetti, "Right-handed charged currents in the era of the Large Hadron Collider," *JHEP* **05** (2017) 086, arXiv:1703.04751 [hep-ph].

[45] E. da Silva Almeida, A. Alves, N. Rosa Agostinho, O. J. P. Éboli, and M. C. Gonzalez–Garcia, "Electroweak Sector Under Scrutiny: A Combined Analysis of LHC and Electroweak Precision Data," *Phys. Rev.* **D99** (2019) no. 3, 033001, arXiv:1812.01009 [hep-ph].

[46] T. Corbett, O. J. P. Éboli, and M. C. Gonzalez-Garcia, "Unitarity Constraints on Dimension-six Operators II: Including Fermionic Operators," *Phys. Rev.* **D96** (2017) no. 3, 035006, arXiv:1705.09294 [hep-ph].

[47] A. Butter, O. J. P. Éboli, J. Gonzalez-Fraile, M. C. Gonzalez-Garcia, T. Plehn, and M. Rauch, "The Gauge-Higgs Legacy of the LHC Run I," *JHEP* **07** (2016) 152, arXiv:1604.03105 [hep-ph].

[48] K. Hagiwara, R. D. Peccei, D. Zeppenfeld, and K. Hikasa, "Probing the Weak Boson Sector in e+ e- —> W+ W-," *Nucl. Phys.* **B282** (1987) 253–307.

[49] R. Alonso, M. B. Gavela, L. Merlo, S. Rigolin, and J. Yepes, "The Effective Chiral Lagrangian for a Light Dynamical "Higgs Particle"," *Phys. Lett.* **B722** (2013) 330–335, arXiv:1212.3305 [hep-ph]. [Erratum: Phys. Lett.B726,926(2013)].

[50] G. Buchalla, O. Catà, and C. Krause, "Complete Electroweak Chiral Lagrangian with a Light Higgs at NLO," *Nucl. Phys.* **B880** (2014) 552–573, arXiv:1307.5017 [hep-ph]. [Erratum: Nucl. Phys.B913,475(2016)].

[51] M. B. Gavela, J. Gonzalez-Fraile, M. C. Gonzalez-Garcia, L. Merlo, S. Rigolin, and J. Yepes, "CP violation with a dynamical Higgs," *JHEP* **10** (2014) 044, arXiv:1406.6367 [hep-ph].

[52] I. Brivio, J. Gonzalez-Fraile, M. C. Gonzalez-Garcia, and L. Merlo, "The complete HEFT Lagrangian after the LHC Run I," *Eur. Phys. J.* **C76** (2016) no. 7, 416, arXiv:1604.06801 [hep-ph].

[53] **SLD Electroweak Group, DELPHI, ALEPH, SLD, SLD Heavy Flavour Group, OPAL, LEP Electroweak Working Group, L3** Collaboration, S. Schael *et al.*, "Precision electroweak measurements on the Z resonance," *Phys. Rept.* **427** (2006) 257–454, arXiv:hep-ex/0509008 [hep-ex].

[54] **Particle Data Group** Collaboration, M. Tanabashi *et al.*, "Review of Particle Physics," *Phys. Rev.* **D98** (2018) no. 3, 030001.

[55] J. de Blas, M. Ciuchini, E. Franco, S. Mishima, M. Pierini, L. Reina, and L. Silvestrini, "The Global Electroweak and Higgs Fits in the LHC era," *PoS* **EPS-HEP2017** (2017) 467, arXiv:1710.05402 [hep-ph].

[56] D. Zeppenfeld, R. Kinnunen, A. Nikitenko, and E. Richter-Was, "Measuring Higgs boson couplings at the CERN LHC," *Phys. Rev.* **D62** (2000) 013009, arXiv:hep-ph/0002036 [hep-ph].

[57] M. Duhrssen, S. Heinemeyer, H. Logan, D. Rainwater, G. Weiglein, and D. Zeppenfeld, "Extracting Higgs boson couplings from CERN LHC data," *Phys. Rev.* **D70** (2004) 113009, arXiv:hep-ph/0406323 [hep-ph].

[58] R. Lafaye, T. Plehn, M. Rauch, D. Zerwas, and M. Duhrssen, "Measuring the Higgs Sector," *JHEP* **08** (2009) 009, arXiv:0904.3866 [hep-ph].

[59] A. Butter, *Global Fits for New Physics at the LHC and Beyond*. PhD thesis, U. Heidelberg (main), 2017. http://www.thphys.uni-heidelberg.de/~plehn/includes/theses/butter_d.pdf.

[60] K. Cranmer, "Practical Statistics for the LHC," in *Proceedings, 2011 European School of High-Energy Physics (ESHEP 2011): Cheile Gradistei, Romania, September 7-20, 2011*, pp. 267–308. 2015. arXiv:1503.07622 [physics.data-an]. [,247(2015)].

[61] T. Plehn, "Lectures on LHC Physics," *Lect. Notes Phys.* **844** (2012) 1–193, arXiv:0910.4182 [hep-ph].

[62] G. Cowan, *Statistical data analysis*. 1998.

[63] J. Neyman and E. S. Pearson, "On the Problem of the Most Efficient Tests of Statistical Hypotheses," *Philosophical Transactions of the Royal Society of London* **A231** (1933) 289–337.

[64] G. Cowan, K. Cranmer, E. Gross, and O. Vitells, "Asymptotic formulae for likelihood-based tests of new physics," *Eur. Phys. J.* **C71** (2011) 1554, arXiv:1007.1727 [physics.data-an]. [Erratum: Eur. Phys. J.C73,2501(2013)].

[65] S. S. Wilks, "The Large-Sample Distribution of the Likelihood Ratio for Testing Composite Hypotheses," *Annals Math. Statist.* **9** (1938) no. 1, 60–62.

[66] A. Wald, "Tests of statistical hypotheses concerning several parameters when the number of observations is large," *Transactions of the American Mathematical Society* **54** (1943) no. 3, 426–482.

[67] W. Verkerke and D. P. Kirkby, "The RooFit toolkit for data modeling," *eConf* **C0303241** (2003) MOLT007, arXiv:physics/0306116 [physics]. [,186(2003)].

[68] F. James and M. Winkler, "MINUIT User's Guide,".

[69] A. A. Markov, "Rasprostranenie zakona bol'shih chisel na velichiny, zavisyaschie drug ot druga," *Izvestiya Fiziko-matematicheskogo obschestva pri Kazanskom universitete* **15** (1906) no. 135-156, 18.

[70] B. C. Allanach and C. G. Lester, "Multi-dimensional mSUGRA likelihood maps," *Phys. Rev.* **D73** (2006) 015013, arXiv:hep-ph/0507283 [hep-ph].

[71] R. Lafaye, T. Plehn, M. Rauch, and D. Zerwas, "Measuring Supersymmetry," *Eur. Phys. J.* **C54** (2008) 617–644, arXiv:0709.3985 [hep-ph].

[72] N. Metropolis, A. W. Rosenbluth, M. N. Rosenbluth, A. H. Teller, and E. Teller, "Equation of state calculations by fast computing machines," *The Journal of Chemical Physics* **21** (1953) no. 6, 1087–1092. http://link.aip.org/link/?JCP/21/1087/1.

[73] W. K. Hastings, "Monte carlo sampling methods using markov chains and their applications," *Biometrika* **57** (1970) no. 1, 97–109, http://biomet.oxfordjournals.org/cgi/reprint/57/1/97.pdf. http://biomet.oxfordjournals.org/cgi/content/abstract/57/1/97.

[74] A. Corana, M. Marchesi, C. Martini, and S. Ridella, "Minimizing multimodal functions of continuous variables with the "simulated annealing" algorithm—corrigenda for this article is available here,"*ACM Trans. Math. Softw.* **13** (Sept., 1987) 262–280. http://doi.acm.org/10.1145/29380.29864.

[75] M. Dittmar *et al.*, "Parton Distributions," arXiv:0901.2504 [hep-ph].

[76] J. Gao, L. Harland-Lang, and J. Rojo, "The Structure of the Proton in the LHC Precision Era," *Phys. Rept.* **742** (2018) 1–121, arXiv:1709.04922 [hep-ph].

[77] N. P. Hartland, F. Maltoni, E. R. Nocera, J. Rojo, E. Slade, E. Vryonidou, and C. Zhang, "A Monte Carlo global analysis of the Standard Model Effective Field Theory: the top quark sector," arXiv:1901.05965 [hep-ph].

[78] Z. Zhang, "Time to Go Beyond Triple-Gauge-Boson-Coupling Interpretation of W Pair Production," *Phys. Rev. Lett.* **118** (2017) no. 1, 011803, arXiv:1610.01618 [hep-ph].

[79] J. Baglio, S. Dawson, and I. M. Lewis, "An NLO QCD effective field theory analysis of W^+W^- production at the LHC including fermionic operators," *Phys. Rev.* **D96** (2017) no. 7, 073003, arXiv:1708.03332 [hep-ph].

[80] J. Baglio, S. Dawson, and I. M. Lewis, "NLO effects in EFT fits to W^+W^- production at the LHC," *Phys. Rev.* **D99** (2019) no. 3, 035029, arXiv:1812.00214 [hep-ph].

[81] A. Alves, N. Rosa-Agostinho, O. J. P. Éboli, and M. C. Gonzalez-Garcia, "Effect of Fermionic Operators on the Gauge Legacy of the LHC Run I," *Phys. Rev.* **D98** (2018) no. 1, 013006, arXiv:1805.11108 [hep-ph].

[82] S. Dawson and A. Ismail, "Standard model EFT corrections to Z boson decays," *Phys. Rev.* **D98** (2018) no. 9, 093003, arXiv:1808.05948 [hep-ph].

[83] J. Ellis, C. W. Murphy, V. Sanz, and T. You, "Updated Global SMEFT Fit to Higgs, Diboson and Electroweak Data," *JHEP* **06** (2018) 146, arXiv:1803.03252 [hep-ph].

[84] A. Biekötter, T. Corbett, and T. Plehn, "The Gauge-Higgs Legacy of the LHC Run II," arXiv:1812.07587 [hep-ph].

[85] F. Krauss, S. Kuttimalai, and T. Plehn, "LHC multijet events as a probe for anomalous dimension-six gluon interactions," *Phys. Rev.* **D95** (2017) no. 3, 035024, arXiv:1611.00767 [hep-ph].

[86] A. Buckley, C. Englert, J. Ferrando, D. J. Miller, L. Moore, M. Russell, and C. D. White, "Constraining top quark effective theory in the LHC Run II era," *JHEP* **04** (2016) 015, arXiv:1512.03360 [hep-ph].

[87] I. Brivio and M. Trott, "The Standard Model as an Effective Field Theory," arXiv:1706.08945 [hep-ph].